# Hybrid islanding detection technique for single-phase grid-connected photovoltaic multi-inverter systems

Barkat, Fadila; Cheknane, Ali; Guerrero, Josep M.; Lashab, Abderezak; Istrate, Marcel; Viorel, Ioan

*Published in:*
IET Renewable Power Generation

*DOI (link to publication from Publisher):*
10.1049/iet-rpg.2019.1183

*Publication date:*
2021

*Document Version*
Accepted author manuscript, peer reviewed version

# A Hybrid Islanding Detection Technique for Single-Phase Grid-Connected Photovoltaic Multi-Inverter Systems

Fadila Barkat[1], Ali Cheknane[1], Josep M. Guerrero[2*], Abderezak Lashab[2], Marcel Istrate[3], Ioan Viorel Banu[3]

[1] Laboratoire des Semiconducteurs et Matériaux Fonctionnels, Université Amar Telidji de Laghouat, Bd des Martyrs BP37G, Laghouat-03000, Algerie
[2] Center for Research on Microgrids (CROM), Department of Energy Technology, Aalborg University (AAU), Denmark
[3] Power Engineering Department, "Gheorghe Asachi" Technical University of Iasi, Romania
[*] joz@et.aau.dk

**Abstract: This paper presents the performance of a novel hybrid islanding detection method (IDM) for multi-single-phase photovoltaic (PV) inverters based on the combination of four active methods and three passive methods. Although islanding detection in PV multi-inverter systems has been widely researched, most islanding studies are focused on three-phase inverters, rather than single-phase ones. In this paper, different active and passive methods are used to detect the islanding of four paralleled single-phase PV inverters. By combining those methods synergistically, it reduces their weakness of each method, while combining their advantages. The novelty of the proposed system methodology consists of four paralleled single-phase inverters equipped with four different active methods, named Active Frequency Drift (AFD), Sandia Frequency Shift (SFS), Sliding Mode frequency Shift (SMS), and Sandia Voltage Shift (SVS) triggered by a block composed by three passive methods: voltage frequency protection (VFP), rate of change of frequency (ROCOF), and DC-link. This novel hybrid system is studied under different detailed scenarios, where it shows its performance and characteristics.**

## 1 Introduction

Islanding is a condition in which a part of the utility system containing both load and distributed generations (DGs) remains stimulated while disconnected from the rest of the utility grid [1, 3]. The islanding detection is an obligatory element for the photovoltaic (PV) inverters as indicated in global standards and rules [1].

### *1.1 Motivation and Incitement*

There are passive and active islanding detection methods (IDMs) [4, 63]. Major parts of PV inverters controller consist of a maximum power point tracker (MPPT) and a current control loop, while utilizing passive islanding detection strategies based on estimated parameters. Under islanding conditions, the voltage and frequency at the point of common coupling (PCC) tend to go out from the acceptable window when unbalances in active and reactive power occur. Passive under/over-frequency protection (UFP/OFP) and under/over-voltage protection (UVP/OVP) is compelling in anticipating islanding in systems with sufficiently low power [4].

The above mentioned IDMs are not complex and they present reliable results [39]. However, at the same time, they present large non-detection zones (NDZs) where they cannot detect the islanding condition [4]. Furthermore, with the large expansion of PV systems, it is likely that energy/geographical islands or microgrids will contain different inverters. Therefore, it is necessary to investigate the impact of active IDMs when they are applied to multi-inverter systems.

### *1.2 Literature Review*

An overview of the existing IDMs can be found in [43, 44] and [45]. Many IDMs have been presented in the literature such as passive IDMs [46-48], active IDMs [49-51] and [52, 53], which are based on phase-locked loop (PLL), impedance-based measurements IDMs [54, 55], and hybrid IDMs [41, 42] and [56, 57]. Other reported techniques were used for islanding detection in DG [58-61] or in PV-based microgrids (MGs) [62]. In [63-65] were presented other IDMs for PV systems.

In [40], a hybrid IDM combination of Sliding Mode frequency Shift (SMS) and reactive power versus frequency (Q-f) as active methods, and UFP/OFP as passive methods have been proposed. In [66] a hybrid method based on the optimized Sandia Frequency Shift (SFS) method as the selected active method, in combination and coordination of rate of change of frequency (ROCOF) and UFP/OFP relays as the passive methods is discussed.

The literature [4, 5] shows that active IDMs can reduce the NDZ of passive techniques in single-inverter systems. However, systems with different inverters, equipped with active IDMs, need to be more researched to study the interference of the methods integrated in DG inverters [4, 5].

Therefore, it is necessary to identify the conditions of efficient islanding. To analyse this problem, several approaches have been proposed [6]. New IDMs have been developed from the basic methods such as the improved SMS [11] and modified SFS based artificial immune system techniques [12]. The single- and multi-inverter approaches were studied in [9] and [8], respectively.

Moreover, the performance of a system having two parallel-connected inverters is discussed in [8] and [67] by analysing the NDZs of a combination of frequency drifting methods like: Active Frequency Drift (AFD), SFS, and SMS [67]. In [22], the performance of three grid-tied inverters with its own active IDM [Sandia voltage shift (SVS), SFS, and SMS] and connected in parallel to the same load has been explored. The classical linear instability method (CLIM) of

islanding prevention implemented in the Teslaco multi-inverters is studied in [13], in which the relation between run-on times (ROTs) and the number of inverters is presented [22]. In [5], a small-signal stability analysis of dynamic NDZs of the positive feedback anti-islanding scheme for single- and multi-inverters systems is proposed.

### *1.3 Contribution and Paper Organization*

This paper shows improvement for earlier works. A system with four DG inverters, in which each inverter has its own, separate, and different IDM, is described here. Furthermore, the overall system performance, considering the interaction between these methods, together with the effect of feedback gain on detection time for such a scenario, is described.

In this paper, a novel hybrid IDM is proposed for multi-single-phase PV inverters based on a combination of 4 active and 3 passive methods. The main contribution and the novelty of the proposed hybrid method consist of 4 parallel-connected PV inverters with its own 4 different active methods triggered by 3 passive relays.

Finally, to justify the effectiveness of the proposed IDM, various simulation studies are performed in the Matlab/Simulink platform under different conditions. The numerical simulation results show that the proposed IDM has a faster detection time than other hybrid methods for multi-inverter grid-connected PV systems existing in the literature, significant reduction in NDZ compared to other passive methods, and low impact on the quality factor ($Q_f$).

This paper has the following structure. Section 2 describes the proposed islanding Simulink implementation with all methods used in the paper. In Section 3, the grid-connected PV system (GCPVS) and its proposed IDM are given. Section 4 discusses the theoretical simulation results of islanding conditions that are detected by the proposed combination of IDM.

## 2 Four Applied Active IDMs

Both active and passive methods have weaknesses, e.g., the passive methods have large NDZs [7], while the active methods have undesirable effects on the power quality of the system [1]. Combining these two types of methods involves advantages of both systems and makes it possible to overcome their shortcomings [41, 42, 44, 45, 50, 56].

The proposed system consists of an aggregation of those two kinds of methods with AFD, SFS, SMS, and SVS methods as active methods and hybrid under/over frequency (UOF) and under/over voltage (UOV) method, called Voltage Frequency Protection (VFP), ROCOF, and DC-link as passive ones. All the islanding detection strategies utilized in this paper are described as follows. More details about the different IDMs are presented in Table 1.

The UOF/UOV methods permit the detection of islanding benefit through the proportion of frequency $f_{PCC}$ as well as voltage $V_{PCC}$ [2, 9, 14, 18]. On the off chance that the deliberate qualities are outside the predefined boundaries ($f_{min}$-$f_{max}$) and ($V_{min}$-$V_{max}$). ROCOF relay operations [16-18, 32] are used to recognize islanding DG cases. ROCOF figures the rate of progress of frequency utilizing a portable window more than a few cycles of the voltage waveform. The DC-link protection relay measures the duration time of an electrical cycle and starts a new measurement at each rising zero-crossing of the terminal voltage [17, 18, 32].

As mentioned before, the condition of *"islanding"* in PV systems is an electrical phenomenon that occurs when the energy injected into the power grid is interrupted due to various factors and the PV inverters continue energizing some loads or the entire loads [1]. Thus, the power grid stops controlling this isolated part of the distribution system, which contains both loads and generation [1]. This situation may compromise security, restoration of service, and the reliability of the equipment [1, 14].

**Table 1** Performance comparison of the used IDMs

| Methods | | NDZ | Weaknesses | Advantages |
|---|---|---|---|---|
| *Active methods* | AFD | Relatively large NDZ compared to other IDMs; depends on the used chopping fraction | Small degradation in output power quality | Very easy to implement with microprocessor-based inverter controllers |
| | SMS | small NDZ contrast | Requires a decrease in the output power quality of the PV inverter, albeit a small one | Relatively easy to implement; highly effective in multiple inverters |
| | SFS | NDZ can be made extremely small | Requires that the output power quality reduced slightly; possibility of the instability of the inverter output power | Relatively high Q loads; easy to implement; retains effectiveness with multiple inverters |
| | SVS | Similar NDZ to the standard UOF/UOV methods | Delivers a small reduction in the power quality; might influence the accuracy of MPPT calculations | Easy and viewed as extremely compelling among the positive feedback techniques |
| *Passive methods* | UOF/ UOV | Dependent on impedances, power ratings, and operating point | Low reaction times | Low cost, equivalent to utility protection; are used in conjunction with others IDMs |
| | ROCOF | Large NDZ | Difficult to detect islanding in specific cases | Short detection time; do not perturb the system; accurate when there is a large mismatch in generation |
| | DC-link | Large NDZ | Difficult to detect islanding in specific cases | Short detection time |

The islanding situation of a GCPVS at the PCC is illustrated in Fig. 1. The PCC is situated between the utility grid and a PV DG unit with a local load. The active methods purposefully present aggravations at the output of the inverter to decide whether they influence network voltage, frequency, and impedance parameters [68]. Overall, it is accepted that the power grid has been separated and the inverter winds up segregated from the load [68]. The active methods have the upside of astoundingly lessening or although disposing of the NDZ. In any case, they may weaken the nature of the grid voltages [68].

The standard operation of the SMS technique [11, 21, 22] depends on the fluctuation of the inverter yield frequency by controlling the phase of the inverter current [68]. This strategy is generally simple to execute as it is only a slight alteration of a part, which is now required, the PLL. The SMS method offers a decent trade-off between islanding detection, the output control quality, and momentary reaction [68].

The premise of AFD strategy [23-27] is to fluctuate the frequency of the yield current by methods for a positive input. The strategy is based on the infusion of a current into the PCC somewhat contorted in frequency. At the point when a grid detachment happens, a stage mistake shows up between the inverter current and the voltage at the PCC. The inverter identifies this blunder and attempts to remunerate it by expanding the frequency of the produced current. This procedure proceeds until the point at which the frequency surpasses the breaking points and is recognized by the UFP/OFP. This technique can be effectively actualized and connected to multi-inverters. In any case, the AFD technique creates a small decrease in the nature of the DG yield [68].

The SFS method [10, 12, 21, 22] is a quickened adaptation of the AFD method and it is one of the positive input strategies used to keep the islanding operation. With the lattice associated, the technique distinguishes and acts to enhance small changes in frequency, yet the presence of the grid evades it [68]. Also, the SVS strategy [22, 28] utilizes a positive feedback circle of the PCC voltage adequacy [68]. The SVS and SFS methods improve the performance of the proposed hybrid technique by activating at the same time the frequency and voltage when islanding occurs.

Most common active methods (SMS, SFS, SVS, and AFD) are good, but they are limited by serious weakness especially in multi-inverters cases [8, 10]. To limit this problem, a study based on the superposition of all those four active methods is presented. In this paper, this new proposed system composed of four single-phase PV inverters, placed in parallel and connected to a utility grid via a breaker, is designed.

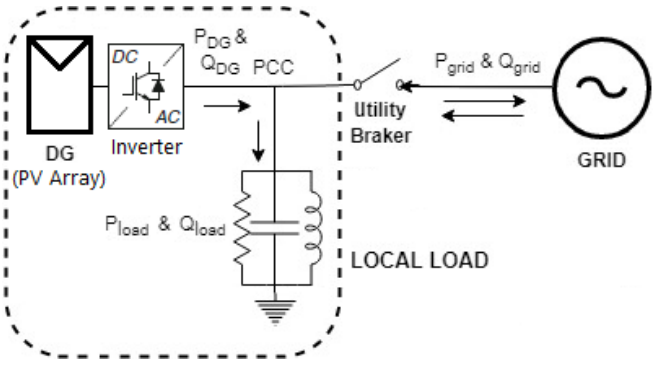


***Fig. 1.*** *Islanding concept for one single-inverter [19-23]*

The grid is supposed to behave as a voltage source ($V_{AC}$) in Fig. 1. A resistive-inductive-capacitive (*RLC*) load is added in parallel to the grid to assess the islanding situation. Each inverter is equipped with these different active methods that are AFD, SFS, SMS, and SVS. Another independent block with three passive methods, namely, ROCOF, DC-link, and a useful hybrid combination method of two passive methods: UOF and UOV methods, called VFP [39] is added to assess the performance of the proposed system by run time and signal response.

## 3 Simulink Implementation of PV Model and Anti-Islanding Methods

Simulation studies are conducted with the MATLAB/Simulink package to evaluate the performance of the proposed method. The 3.5 kW GCPVS, consisting of one string of four PV panels Trina Solar TSM-250PA05.08 [37], is connected to the grid through a full bridge, switching filter, and a low-frequency transformer. The schematic and simulation block of the sample system are shown in Fig. 1 and Fig. 2 respectively. The manufacturer information of the PV panel at 1000 W/m$^2$ radiation and 25°C cell temperature called standard test condition (STC) [37] and the system parameters can be found in Table 2. The PV Panel parameters are extracted from NREL System Advisor Model (Jan. 2014).

**Table 2** PV array and inverter parameters

| | |
|---|---|
| **PV Array Trina Solar TSM-250PA05.08** | |
| Maximum power ($P_m$) | 249.86 W |
| Current at maximum power ($I_m$) | 8.06 A |
| Voltage at maximum power ($V_m$) | 31 V |
| Open-circuit voltage ($V_{oc}$) | 37.6 V |
| Short-circuit current ($I_{sc}$) | 8.55 A |
| Cells per module | 60 |
| Temperature coefficient of $V_{oc}$ | –0.35 (%/) |
| Temperature coefficient of $I_{sc}$ | 0.06 (%/) |
| Number of series modules | 14 |
| Number of parallel strings | 1 |
| **Weather conditions** | |
| Irradiance | 1000 W/m² |
| Temperature | 25°C |
| **DC Voltage Controller** | |
| Proportional gain | 12 |
| Integral gain | 200 |
| **Inverter Control** | |
| Nominal power | 3.5 kW |
| Primary voltage $V_g$ ($V_{RMS}$ LL) | 240 V |
| Frequency | 60 Hz |
| DC voltage | 400 V |
| Carrier frequency | 3780 Hz |
| Output limits | [375–450] V |
| **Current Regulator** | |
| Proportional gain | 0.15 |
| Integral gain | 6.6 |
| **Filter** | |
| Inverter-side inductance filter ($L_i$) | 1.73 mH |
| Grid-side inductance ($L_g$) | 2 mH |
| Capacitance ($C_f$) | 15 µF |

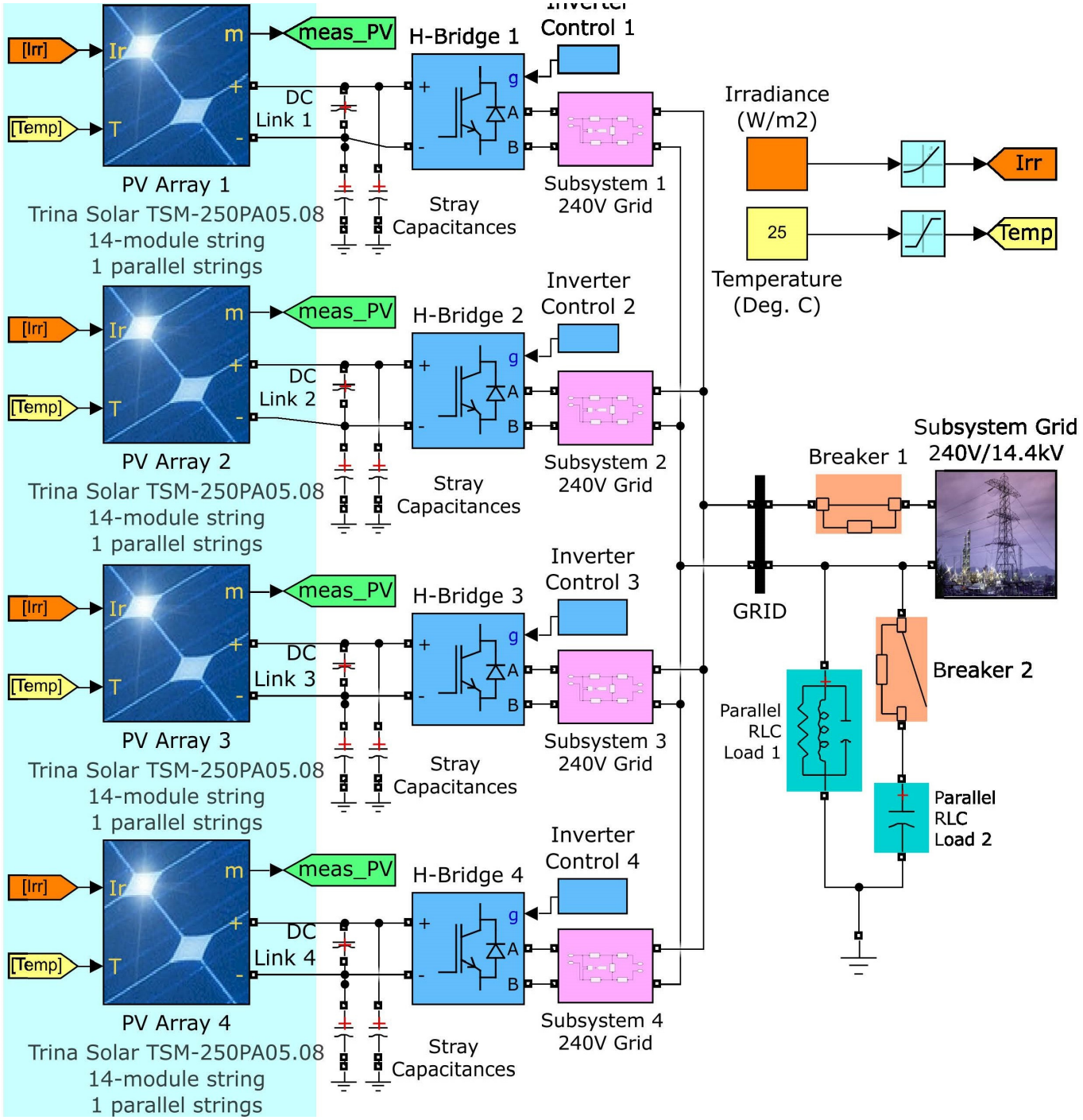


***Fig. 2.*** *Proposed detailed Simulink model of GCPVS*

The islanding condition is simulated in all simulations by opening the circuit breaker shown in Fig. 1, at $t = 0.5$ s.

Furthermore, the simulations are performed under the following conditions:

- Different active power imbalances in the islanded area
- Different quality factors for local load during no active power imbalance condition
- Various types of local load (*R*, *RL*, *RC*, and *RLC*)
- Non-islanding conditions
- Proposed model of inverter control comparing with the same system equipped by the active methods for all inverters in the same time (AFD, SFS, SMS, and SVS inverters)

As shown in Fig. 2, a proposed detailed Simulink model of a GCPVS is modeled and tested for various kinds of active techniques. The reference current created has a changed voltage, frequency, and phase for AFD, SVS, SFS, and SMS techniques separately using Matlab *FUNCTION*. The system parameters are given in Table 2.

The inverter control is built using five major blocks. These blocks are shown in Fig. 3. The first one is the MPPT controller which uses perturb and observe (P&O) method controller to regulate the reference of the DC voltage signal of the inverter to get a DC voltage according to the maximum power from the PV array [73], [74]. Secondly, the $V_{DC}$ regulator determines the required active current (see $i_d$ in Fig.

4) for the current regulator. The current regulator is the third subsystem. It uses the determined active current from the previous step and reactive current, which is here set at 0 A [38], to determine the required reference voltages for the inverter. The next part is the *PLL & Measurements* block. This block ensures the synchronization and the measurement of the voltages and currents. The last part is the pulse width modulation (PWM) generator that generates the carrier frequency for the PWM bipolar modulation to perform the switching of the IGBTs. The control system is based on the [37] model from Simulink and described in detail there.

The instantaneous real and reactive power in terms of the *d-q* axis components for single-phase systems are given in (1) [40]:

$$p = v_{td} \cdot i_{td}; \qquad q = v_{tq} \cdot i_{tq}. \quad (1)$$

The $I_{DG}$ and $V_{PCC}$ are first transferred to $\alpha\beta$-components and then they are transformed into the *d-q* components using the Park transformation. In Fig. 4, the *d-q* components of currents are denoted by $i_{td}$ and $i_{tq}$ and the *d-q* components of voltages are denoted by $v_{td}$ and $v_{tq}$. The $I_{dref}$ controls the active power supplied by the DG, while $I_{qref}$ controls the output reactive power of the DG. With $I_{qref}$ set equal to zero [38], no reactive power is supplied by the DG and the DG operates at unity power factor [22]-[24]. Then, by passing these reference currents through the phase angle transformation, $I^*_{dref}$ and $I^*_{qref}$ are obtained as in (2) [40].

$$\begin{bmatrix} I^*_{d_{ref}} \\ I^*_{q_{ref}} \end{bmatrix} = \begin{bmatrix} \cos\theta_f & -\sin\theta_f \\ \sin\theta_f & \cos\theta_f \end{bmatrix} \begin{bmatrix} I_{d_{ref}} \\ I_{q_{ref}} \end{bmatrix} \quad (2)$$

where $\theta_f = \omega t$ is the phase angle, $\omega$ is the rotational speed of the *d-q* reference frame, and *t* is the time, in seconds (s). The phase angle transformation in (2) is not a part of the basic constant power control but from the implementation of SMS method.

Then, $I^*_{dref}$ and $I^*_{qref}$ are compared with $i_d$ and $i_q$, which are the inverter output currents, and are passed through the current regulator to the outputs $V_{dref}$ and $V_{qref}$. Given (3), the $V_{dref}$ and $V_{qref}$ are transformed to $V_{sd}$ and $V_{sq}$ as [4].

$$\begin{cases} V_{sd} = V_{d_{ref}} + v_{td} - i_q \omega L_f \\ V_{sq} = V_{q_{ref}} + v_{tq} + i_d \omega L_f \end{cases} \quad (3)$$

where $L_f$ is the filter inductance. The inverter terminal voltages $V_{sd}$ and $V_{sq}$ are used to calculate the modulation index amplitude ($m$) and phase angle ($\varphi$), which are calculated from (4) [40]. The PWM strategy is implemented to determine the ON and OFF signals of the inverter switches [40]. It is also possible to have a more robust controller, to be used such as predictive-based approach model [24]-[27]. This type of interface can control the DG active and reactive output power [40].

$$m = \sqrt{V^2_{d_{ref}} + V^2_{q_{ref}}}; \qquad \varphi = \tan^{-1}\frac{V_{q_{ref}}}{V_{d_{ref}}}. \quad (4)$$

An inverter fed by a PV array is connected to the utility grid through an *LCL* filter to attenuate the current harmonics. In this grid-connected mode, the inverter output current should be controlled to supply power to the grid within the allowable distortion range of current [14]. In the event of any grid faults or intentional switchover, the inverter must operate as a voltage source to supply power to the local load under islanded mode [6].

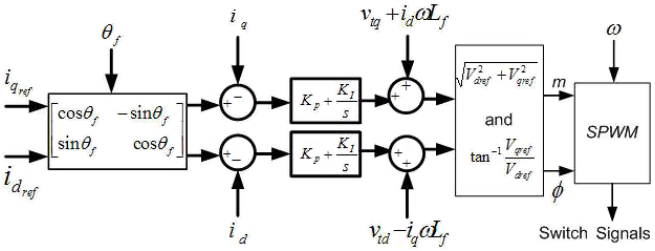


***Fig. 4.*** *DG interface control for constant power operation*

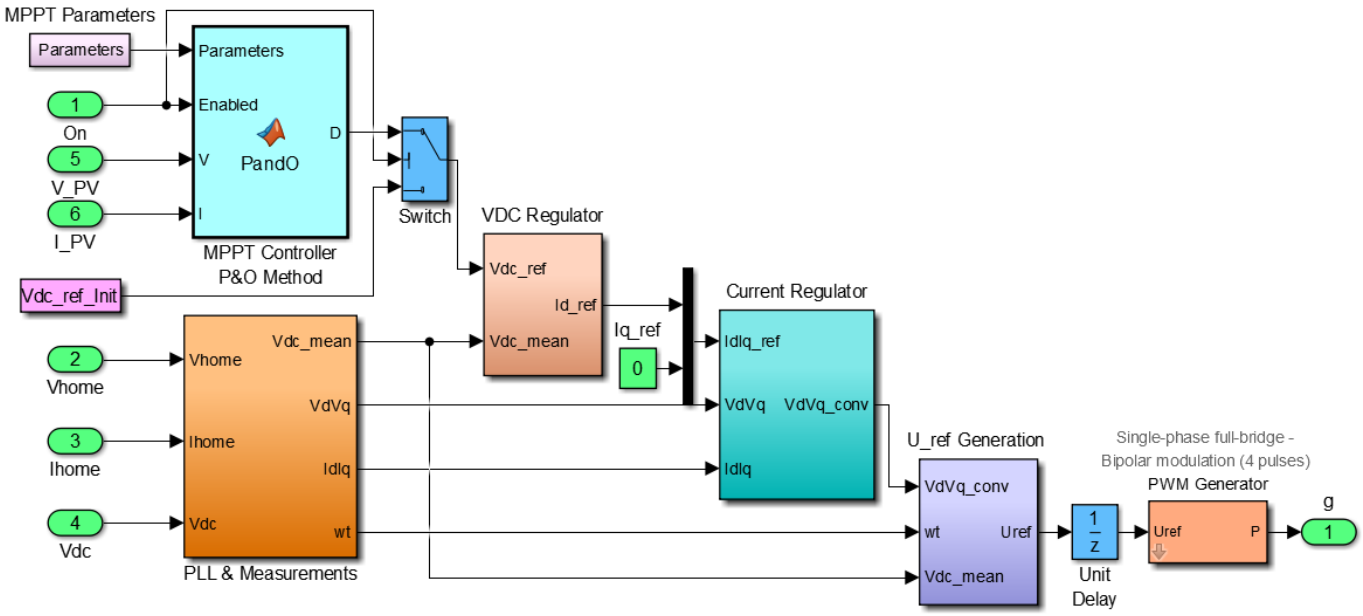


***Fig. 3.*** *Inverter control system*

The proposed model involves four single-stage inverters associated in parallel to a similar load, where every inverter destabilizes one component of the PCC voltage amplitude, frequency, and phase by infusing an altered current to the PCC. The matrix tied multi-inverter requires the grid-connected inverter to stop stimulating inside 2 s in an islanding condition, if the PCC voltage surpasses any of the permitted edges: $V_{max} = 110\ \%$ and $V_{min} = 88\ \%$ of the apparent voltage. Furthermore, if the frequency overpasses the edges: $f_{max} = 60.5$ Hz and $f_{min} = 59.3$ Hz, the inverter should stop in less than 2 s [1]. The greatest AFD, SFS, SVS, and SMS methods associated with a resounding *RLC* stack with the quality factor $Q_f = 2.5$, as required by task and system interconnected standards IEEE Std. 1547 and IEC Std. 62116. Besides, IEC Std. 61727 squares with 5 % of perceived current [24]. The voltage yields of the current controller are changed over to adjusting signals $U_{ref}$ utilized by the PWM generator.

The Simulink models of ROCOF and DC-link methods from [3] present the frequency and the terminal voltage of the PV inverter. In the present work, the ROCOF security screens compares the frequency of the PV inverter with a specific end goal to figure out the ROCOF that is contrasted and the ROCOF limit [32]. The frequency for the ROCOF relay is assessed by a PLL estimator [3], [32]. The parameters of the used anti-islanding methods are summarized in Table 3, where $f$ is the frequency of utility voltage, $\theta_m$ is the maximum phase angle, $f_m$ - $f_g$ is the frequency difference, $f_m$ is the frequency at which the maximum phase shift $\theta_m$ occurs, $K_v$ is the voltage gain (The response time of the SVS algorithm can be adjusted by a factor $K_v$.), $cf_0$ is the initial chopping fraction, $K_f$ is the SFS accelerating frequency gain, and $V_t$ is the terminal voltage of PV inverter.

The VFP method from [32] is a basic passive method, which must be found in any islanding system. The VFP method takes care of the comparison between the existing signal (current, voltage, or frequency) by the thresholds given and denoted by standards and trips the system if any surpass is occurring. The VFP method is very effective but like all passive methods suffer from the NDZ problem. This last will be resolved by using many active methods in parallel and studying their performance together.

Every time and regardless of the entire tested Simulink scenario in this work, a relay statue is given. Fig. 5 gives an example of the relay status used in all the work simulation. As shown in Fig. 5, the results for an *RLC* local load using UOF/UOV, ROCOF, and DC-link methods for the $Q_f = 1$ case are presented in frequency and voltage to switch off the system after some tenths of a second due to the assumed protection scheme used by the local utility.

**Table 3** Simulated parameters of the used IDMs

| | Methods | Parameters |
|---|---|---|
| *Active methods* | AFD | $\delta f = 1.5$ Hz |
| | SMS | $\theta_m = 25°, f_m - f_g = 3$ Hz |
| | SVS | $K_v = 0.3$ |
| | SFS | $cf_0 = 0.05, K_f = 0.05$ |
| *Passive methods* | UOF/UOV | $f_{min} = 59.3$ Hz, $V_{max} = 110\ \%\ V_g$<br>$f_{max} = 60.5$ Hz, $V_{min} = 88\ \%\ V_g$ |
| | ROCOF | $V_t(pu) = 1.043$<br>ROCOF threshold = 5 Hz/s |
| | DC-link | DC-link voltage threshold = 440 V |

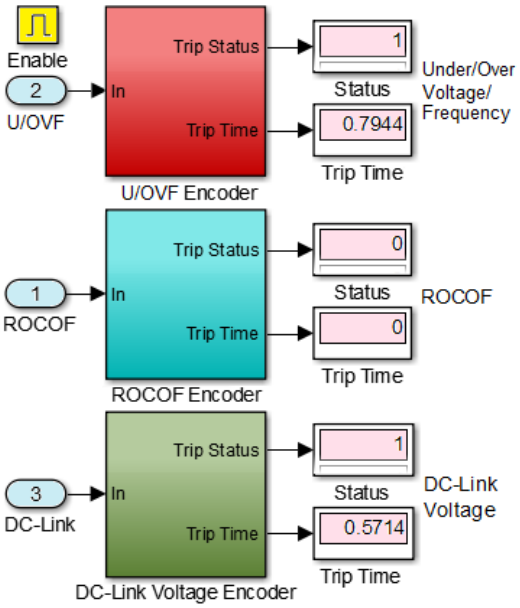


***Fig.* 5.** *Relay status and trip time of IDMs (case of a system with RLC local load, $Q_f = 2.5$, and 250 W/m² irradiance)*

For this study, it is assumed that the PV inverters are considered for autonomous operation at the planning stage. This implies that all used PV inverters in this study have the capability by working together for each case study within the range of their active power to supply the total load in the islanded part of the electrical network without affecting the island desirable operational voltage and frequency limits.

## 4 Results and Discussion

In this section, some test results are shown to illustrate the effectiveness of the discussed anti-islanding prevention scheme. The DG units should have the capability to rapidly contribute in supporting the voltage stability by exchanging additional reactive power with the grid within the generator current injection limits and that could introduce an increased risk of failure in detecting islanding operation conditions [25].

The islanding condition is created by opening the switch at the time $t = 0.5$ s to disconnect the whole system from the grid. The frequency is obtained from the PLL block and the frequency deviations are obtained from the ROCOF block of the proposed system.

Fig. 6 presents the $I_{RMS}$ currents at the PCC of the conventional system without active methods, as well as the proposed system. The effect of the proposed algorithm is clearly emphasized in Fig. 6 by comparing with the conventional curves without any methods. Each active method has a special performance. The zoomed view presents that each inverter equipped with proposed active IDMs give a different interaction.

### *4.1 Analysis of Non-Detection Zone*

In this section, the investigation of the interaction among multiple inverters and the corresponding NDZ will be performed with the help of phase criteria [21, 70]. The conventional phase criterion is a powerful tool to analyse the islanding operation of inverters equipped with active and passive anti-islanding schemes.

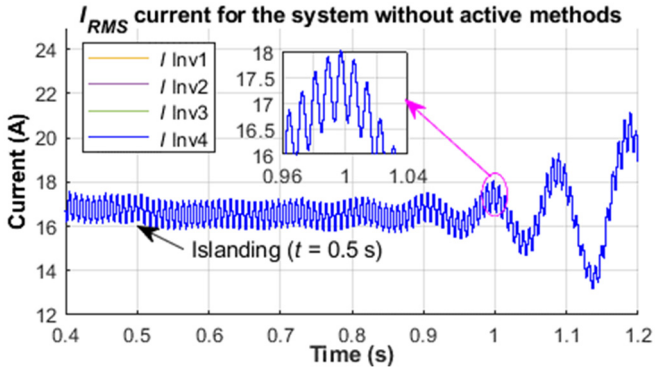


*a*

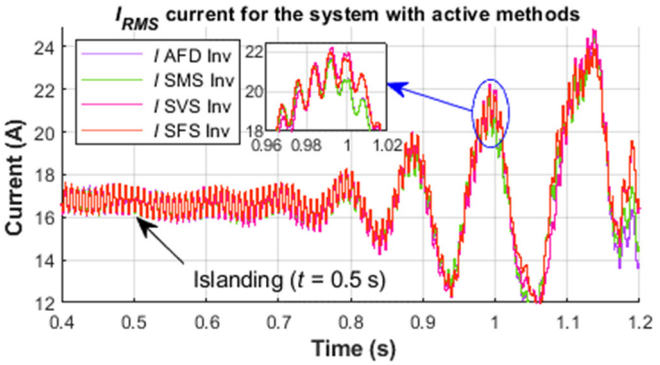


*b*

***Fig. 6.*** *Simulation of $I_{RMS}$ outputs in the PCC point*
*a* Conventional system without active methods and
*b* Proposed system

The equivalent phase angle of the total inverter currents will be derived and utilized to map the NDZs. Inverters operating in parallel can be replaced by an equivalent power conditioning system (PCS) whose capacity is the same to all inverters and the NDZ of parallel PCSs can be easily identified through this equivalent PCS [71].

By the results in Fig. 7, the NDZ of multiple-inverters can be analysed using trigonometric functions to find the phase angle to apply the phase criteria as in [21]. The analysis of NDZ of the proposed system by calculating the phase of the equivalent PCS is given by the coming power ratio of each PCS to the whole PCSs and is defined as the weighting factor $\omega_i$ ($i$ = 1, 2, 3, 4). Then, the resulting formula are presented in (11) in the Appendix section. By considering $\omega = \omega_1 = \omega_2 = \omega_3 = \omega_4$, then will result (12)–(14) from the Appendix section. For each AFD inverter, $\varphi$ can be calculated as in [21, eq. (8)]. Similarly, for SMS and SFS methods as in [21, eq. (12)] and [21, eq. (19)], respectively. The NDZ is plotted using the function of the resonant frequency of the *RLC* load from [72, eq. (33)].

All parameters used in this study are given in Table 3. For the analysis of SVS inverters, the reactive power of the load has a negligible effect on the operation of the SVS method [19]. It applies positive feedback to the amplitude of $V_{PCC}$ and has no effect on phase angle. Then, the phase angle will be considered equal to zero.

The NDZ for the studied method is acquired by calculating the frequency as a function of the quality factor $Q_f$. The boundaries of the NDZ are plotted by replacing the values of $f_{is}$ in [72, eq. (33)] by $f_{max}$ and $f_{min}$, respectively.

Fig. 7 shows the NDZ of equivalent studied systems with different operating frequencies ($f$ = 60.5 Hz / $f$ = 59.3 Hz) respectively. For $Q_f < 2.8$, the proposed system has no NDZ and can detect islanding correctly. For $Q_f = 2.5$, the system is in the safe region of false tripping. The proposed method has a similar NDZ with UOF for high $Q_f$.

### *4.2 Non-Detection Zone Identification*

According to [4] the calculation of the NDZ of a system results in the next formula:

$$\left(\frac{V}{V_{max}}\right)^2 - 1 \le \frac{\Delta P}{P} \le \left(\frac{V}{V_{min}}\right)^2 - 1 \quad (5)$$

$$Q_f\left(1 - \left(\frac{f}{f_{min}}\right)^2\right) \le \frac{\Delta Q}{P} \le Q_f\left(1 - \left(\frac{f}{f_{max}}\right)^2\right) \quad (6)$$

where $V_{max}$, $V_{min}$, $f_{max}$, and $f_{min}$ are under/over voltage and under/over frequency NDZ boundaries, respectively. Typically, $V_{max}$ = 110 % V, $V_{min}$ = 88% V, $f_{max}$ = 60.5 Hz, $f_{min}$ = 59.3 Hz, and $Q_f$ = 2.5. Then [4]:

$$-17.36\ \% \le \frac{\Delta P}{P} \le 29.13\ \% \quad (7)$$

$$-5.94\ \% \le \frac{\Delta Q}{P} \le 4.11\ \% \quad (8)$$

In addition, there is an important relation between $V_{PCC}$, $P_{DG}$, and $Q_{DG}$ as follows [36]:

$$P_{DG} - \Delta P = Real\left({V_{PCC}}^2 / Z_l\right) \quad (9)$$

$$Q_{DG} - \Delta Q = Imag\left({V_{PCC}}^2 / Z_l\right) \quad (10)$$

where $Z_l$ is the load impedance. If $\Delta P$ changes in a positive direction ($P_{load} < P_{DG}$), then the voltage will increase after the breaker opening. Contrariwise, in negative power mismatch ($P_{load} > P_{DG}$), the $V_{PCC}$ will decrease.

In this case study, several sensitive scenarios with the low active/reactive power mismatch have been tested to evaluate the performance of the proposed method under various power mismatch, ranging from 5 % to 30 %. The details of the studied cases are recorded in Table 4.

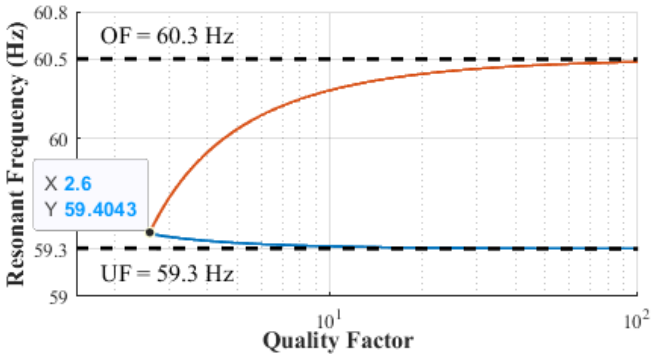


***Fig. 7.*** *NDZ of the proposed method*

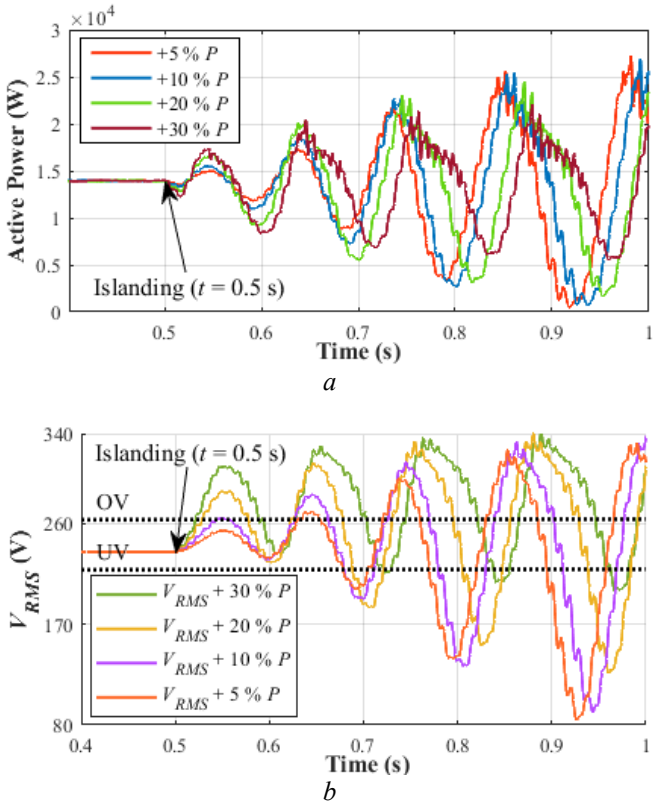


***Fig. 8.*** *Output result of powers and voltages in PCC for:*
*a* Different power imbalance increasing, and
*b* Voltages

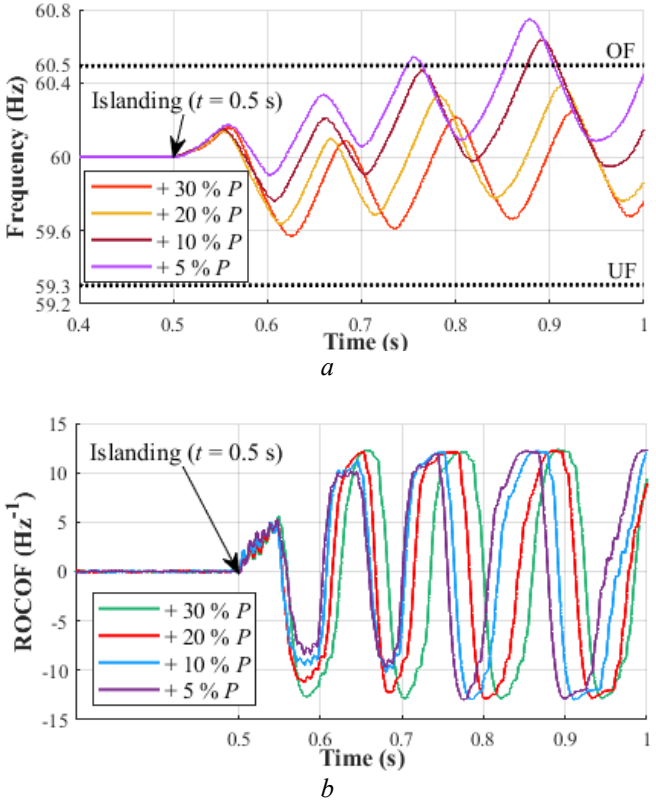


***Fig. 9.*** *Frequency and ROCOF for scenario I*
*a* Frequency, and
*b* ROCOF

### *4.2.1 Scenario I*

In this scenario, the active power mismatch is increased gradually to monitor the voltage, frequency, and ROCOF behaviour of the network, and companion them.

As it is shown in Fig. 8 and Fig. 9, the changes in voltage and frequency are barely noticeable and cannot be detected by relays. However, based on the first scenario, the proposed algorithm can clearly detect islanding with high accuracy in less than 148 ms by VFP relay, from 180 to 280 ms by ROCOF relay, and from 54 to 150 ms when the DC-link relay is applied, as shown in Table 4.

### *4.2.2 Scenario II*

In this scenario, the active power mismatch is decreased to survey the behaviour of the network the same as the previous scenario, as depicted in Fig. 10, and Fig. 11.

**Table 4** Detection time (ms) of the proposed system under islanding for scenarios I and II, applying passive IDMs

| Scenario | Cases | Type of load | VFP | ROCOF | DC-link |
|---|---|---|---|---|---|
| *Scenario I* | Case 1 | +5 % *P* | 148.5 | 281.5 | 254.5 |
| | Case 2 | +10 % *P* | 164.6 | 184.6 | 236.5 |
| | Case 3 | +20 % *P* | 164.6 | 183.7 | 143.9 |
| | Case 4 | +30 % *P* | 164.6 | 199.9 | 54.2 |
| *Scenario II* | Case 1 | -5 % *P* | 248.1 | 37.0 | 108.8 |
| | Case 2 | -10 % *P* | 365.6 | 36.5 | 99.9 |
| | Case 3 | -20 % *P* | 571.0 | 37.5 | 99.5 |
| | Case 4 | -30 % *P* | 685.0 | 38.7 | 106.4 |

The changes in voltage and frequency are barely visible and cannot be detected by relays. By decreasing the active power, the voltage drops at islanding mode in comparison to connected mode.

Since the DG tries to control all parameters, it is difficult to detect islanding based on the changes in voltage and frequency.

However, as depicted in Fig. 10, the proposed algorithm can accurately and efficiently detect the islanding condition under different ranges of mismatched power parameters.

The high accuracy is still achieved in scenario II, when VFP relay disconnect the system in less than 248 ms, around 38 ms by ROCOF relay, and around 100 ms when the DC-link relay is applied, as shown in Table 4.

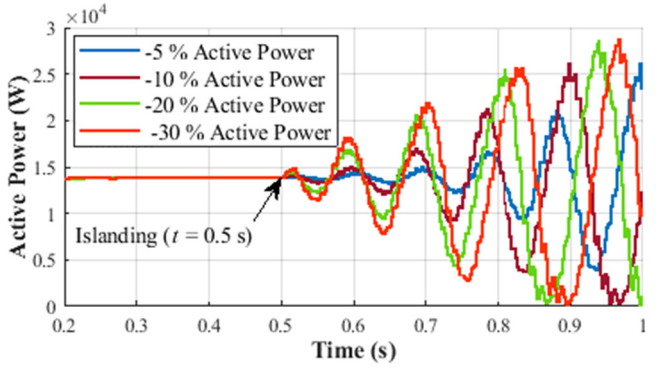


***Fig. 10.*** *Active power at the PCC for different power imbalances decreasing*

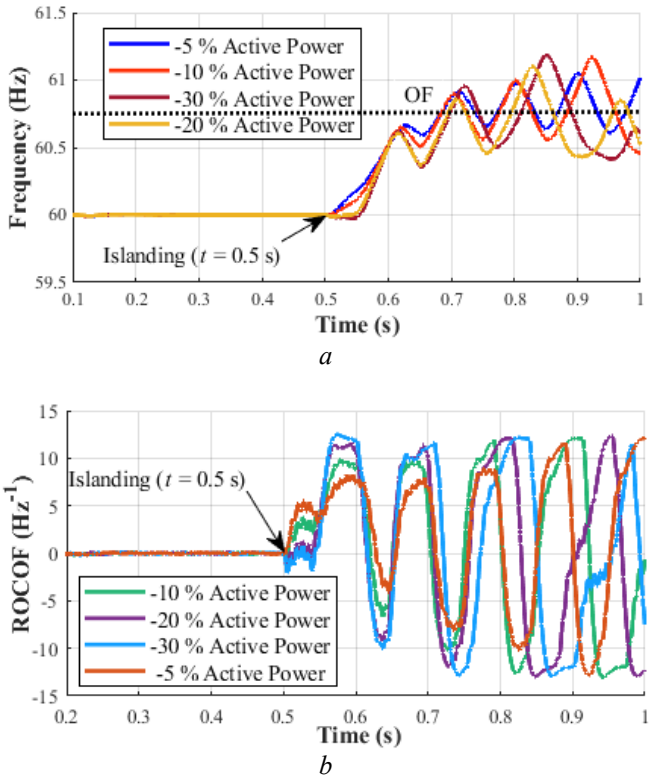


***Fig. 11.*** *Frequency and ROCOF for scenario II*
*a* Frequency, and
*b* ROCOF

### *4.2.3 Scenario III and IV (Q)*

In these scenarios, the reactive power mismatch is increased gradually and the performance of the system is analysed in each part. Fig. 12 shows and compares the network parameters when the reactive power mismatch increases. Although the voltage, output power (Fig. 12), frequency, and ROCOF at PCC (Fig. 13) have some changes in each case, this change is clearer in ROCOF (Fig. 13-*b*) they cannot be detected by relay.

Using the proposed algorithm for islanding condition detection, it accurately detected it in less than 150 ms for VFP method and around 120 ms for ROCOF method. The DC-link method has the longest detection time in these scenarios by a detection time from around 180 ms to 280 ms. Response curves when reactive power decreases are given by presenting the power and voltage in Fig. 14 and frequency and ROCOF variations in Fig. 15. More results are listed in Table 5.

**Table 5** Detection time (ms) of the proposed system with different quality factor and passive IDMs

| | Scenario | Type of load | VFP | ROCOF | DC-link |
|---|---|---|---|---|---|
| *Scenario III* | Case 1 | +5 % $Q$ | 198.2 | 217.5 | 192.3 |
| | Case 2 | +10 % $Q$ | 181.9 | 217.7 | 198.7 |
| | Case 3 | +20 % $Q$ | 198.4 | 218.0 | 275.0 |
| | Case 4 | +30 % $Q$ | 198.5 | 218.5 | 280.6 |
| *Scenario IV* | Case 1 | –5 % $Q$ | 188.1 | 136.2 | 187.0 |
| | Case 2 | –10 % $Q$ | 181.8 | 201.6 | 185.8 |
| | Case 3 | –20 % $Q$ | 181.7 | 119.9 | 185.9 |
| | Case 4 | –30 % $Q$ | 148.5 | 119.4 | 182.8 |

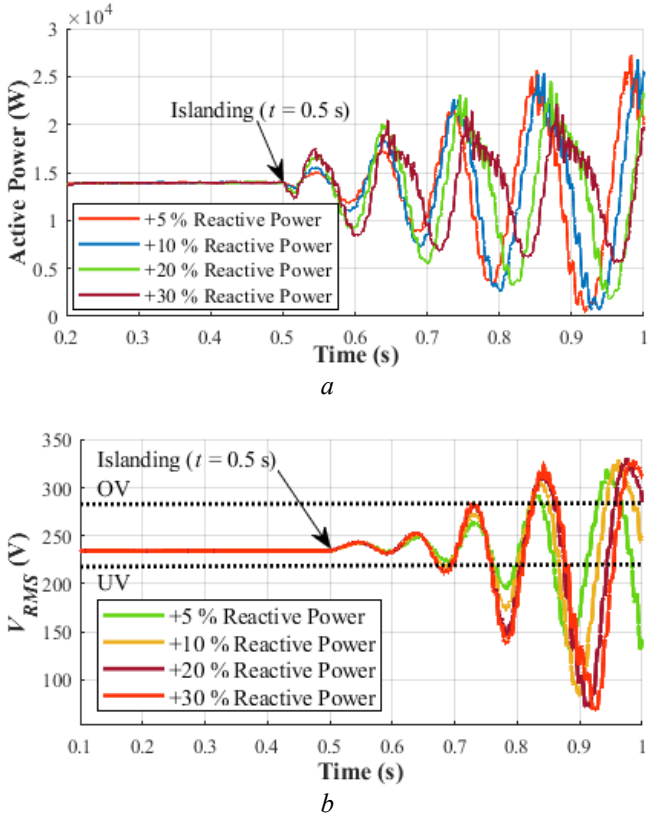


***Fig. 12.*** *Performance of the proposed system at the PCC under different reactive power mismatch increasing*
*a* Active power, and
*b* RMS voltage

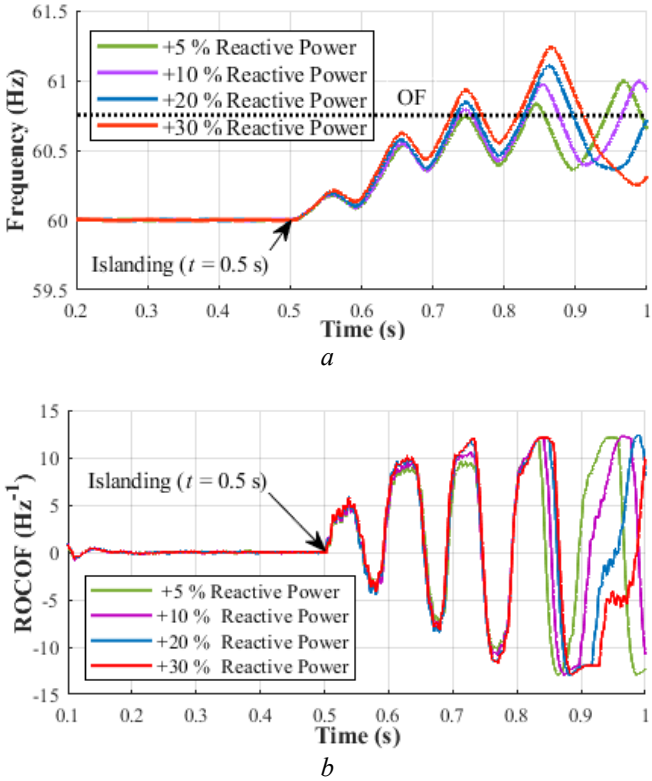


***Fig. 13.*** *Performance of the proposed system at the PCC under different reactive power mismatch increasing*
*a* Frequency (Hz), and
*b* ROCOF (Hz/s)

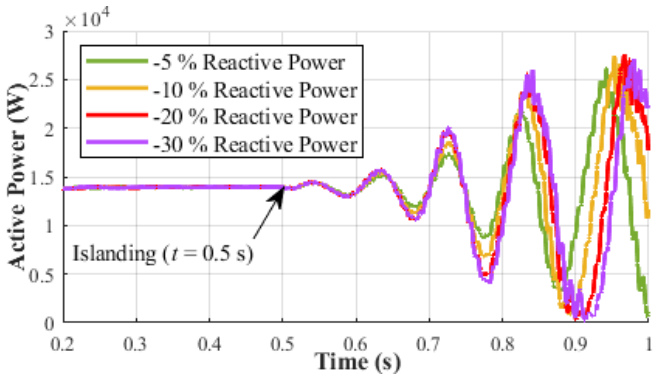


*a*

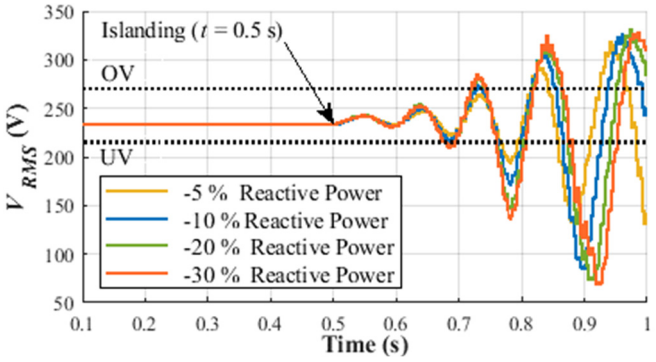


*b*

***Fig. 14.*** *Performance of the proposed system at the PCC under different reactive power mismatch decreasing*
*a* Active power, and
*b* RMS voltage

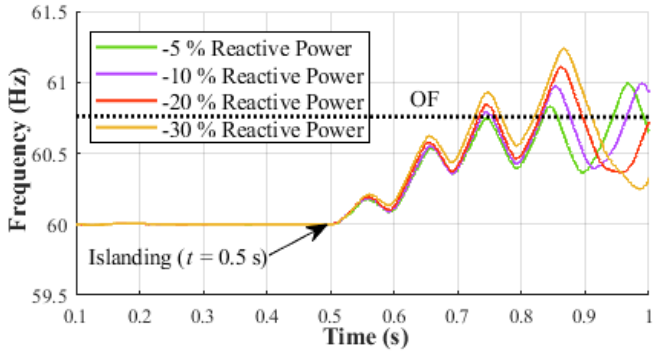


*a*

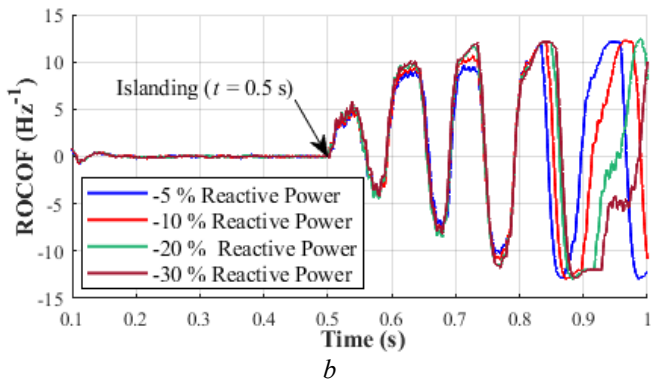


*b*

***Fig. 15.*** *Performance of the proposed system at the PCC under different reactive power mismatch decreasing*
*a* Frequency, and
*b* ROCOF

The dynamic response of the system is studied in four scenarios by observing the change in frequency, voltage, real power, and reactive power for the PCC point and for the grid point across the islanded section, following the transition from grid-connected mode to islanded mode using the load changing islanding power load imbalance strategies. The implementations of these cases are very similar before the islanding occurs. After the disconnection of the utility grid, the reactive power makes some perturbations and destabilization, especially for scenario III. These disturbances have caused deviation.

### *4.3 Influences of Changes in Received Solar Radiations*

All previous cases are studied under 1000 W/m². A study has been proposed to investigate the influence of changes in solar radiation on islanding detection. The simulations are performed in the condition of islanding and partial shading from the beginning of simulations for two cases.

In Fig. 16-*a* the RMS $V_{PCC}$ output voltage during the decrease of received radiation of PV panels from 1000 W/m² to 500 W/m², are illustrated, whereas in the Fig. 16-*b* the $V_{PCC}$ RMS output voltage are presented for the decrease of solar radiation from 500 W/m² to 250 W/m². The obtained results present that the proposed system can deviate from the thresholds of voltage rapidly and therefore the detection by passive methods will be guaranteed. Table 6 lists the performance of the proposed system by indicating the detection time in several cases of power imbalances at different irradiation levels.

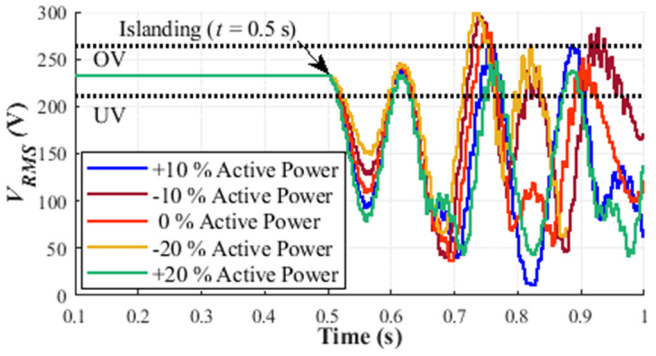


*a*

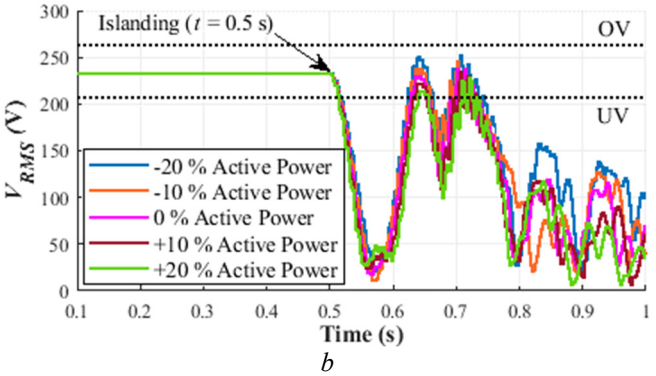


*b*

***Fig. 16.*** *$V_{PCC}$ output voltages for several active power unbalances values at the irradiation level of:*
*a* 500 W/m², and
*b* 250 W/m²

**Table 6** Detection times (ms) for different active power imbalances and different irradiation levels

| Irradiation | $P_D$ | Active power imbalance | VFP | ROCOF | DC-link |
|---|---|---|---|---|---|
| 500 W/m² | 7 kW | 0 % | 316.2 | 235.2 | 55.2 |
| | | +10 % | 292.6 | 260.9 | 53.8 |
| | | +20 % | 282.5 | - | 52.6 |
| | | –10 % | 379.9 | 243.5 | 57.8 |
| | | –20 % | 232.9 | 219.3 | 61.7 |
| 250 W/m² | 3.5 kW | 0 % | 294.4 | - | 71.4 |
| | | +20 % | 283.1 | - | 77.8 |
| | | +10 % | 416.1 | - | 73.7 |
| | | –20 % | 310.2 | 129.3 | 68.7 |
| | | –10 % | 395.4 | - | 69.1 |

### 4.4 Other Islanding Scenarios

This subsection presents the performance of IMDs in case of various load types switching, e.g., load types including constant power, constant current, and constant voltage loads, and the load with different quality factors break down the sustainability of the proposed strategies and to guarantee the detection under different non-islanding conditions.

#### 4.4.1 Influence of Load Types Scenario

There are typical devices and test conditions, each considering an alternate load quality factor, keeping in mind the ultimate goal to test the activity of islanding detection strategies. Different kinds of loads (*R*, *RL*, *RC*, and *RLC*) are used in the following analysis to verify the proposed IDM. The major parameters of this simulation system are according to the standards from [1]. Local load parameters are calculated respecting the relations between *RLC* with $Q_f$ and PV power. Moreover, the voltage of the tested cases is presented in Fig. 18. The parameters of the *RLC* load used in the simulation follow the specified parameters of the IEEE Std. 929-2000 control standard [1] for testing the performance of islanding detection operation. The resonant frequency of the *RLC* load is specified at 60 Hz with a quality factor of 2.5. Limitation from used methods for determining the islanding condition for a 60 Hz system, the allowed frequency ranges for the GCPVS is 59.3–60.5 Hz. Hence, the islanding operation must be detected when the amplitude is over the range of 110 % $V_g$–88 % $V_g$ or the frequency is over the range of 59.3–60.5 Hz.

Fig. 17 presents $I_d$ and $I_q$ variation values of the proposed system in the *R*, *RL*, *RC*, and finally *RLC* load cases. The voltage at PCC and power and the frequency variation for the last cases are presented in Fig. 18. The system for all types of load are similar before the disconnection time. After that, the reaction of each method became clearly different. In addition, the stability of the system is also clearly shown when the system with *RLC* load and $Q_f = 2.5$ have the best

**Table 7** Detection time (ms) of the proposed system with different loads and applying passive IDMs

| Cases | Description | VFP | ROCOF | DC-link |
|---|---|---|---|---|
| 1 | Local load *R*<br>$P = 3500{\cdot}4$ W<br>$Q_C = Q_L = 0$ Var | 74.4 | 36.6 | 104.1 |
| 2 | Local load *RL*<br>$P = 14$ kW<br>$Q_l = 35$ kVar<br>$Q_C = 0$ Var | 53.2 | 43.4 | 38.4 |
| 3 | Local load *RC*<br>$P_{load} = 14$ kW<br>$Q_C = 35$ kVar<br>$Q_L = 0$ Var | 649.0 | 0 | 21.3 |
| 4 | Local load *RLC*<br>with $Q_f = 2.5$<br>$P_{load} = 14$ kW<br>$Q_C = 35$ kVar<br>$Q_L = 35$ kVar | 148.0 | 119.4 | 185.6 |

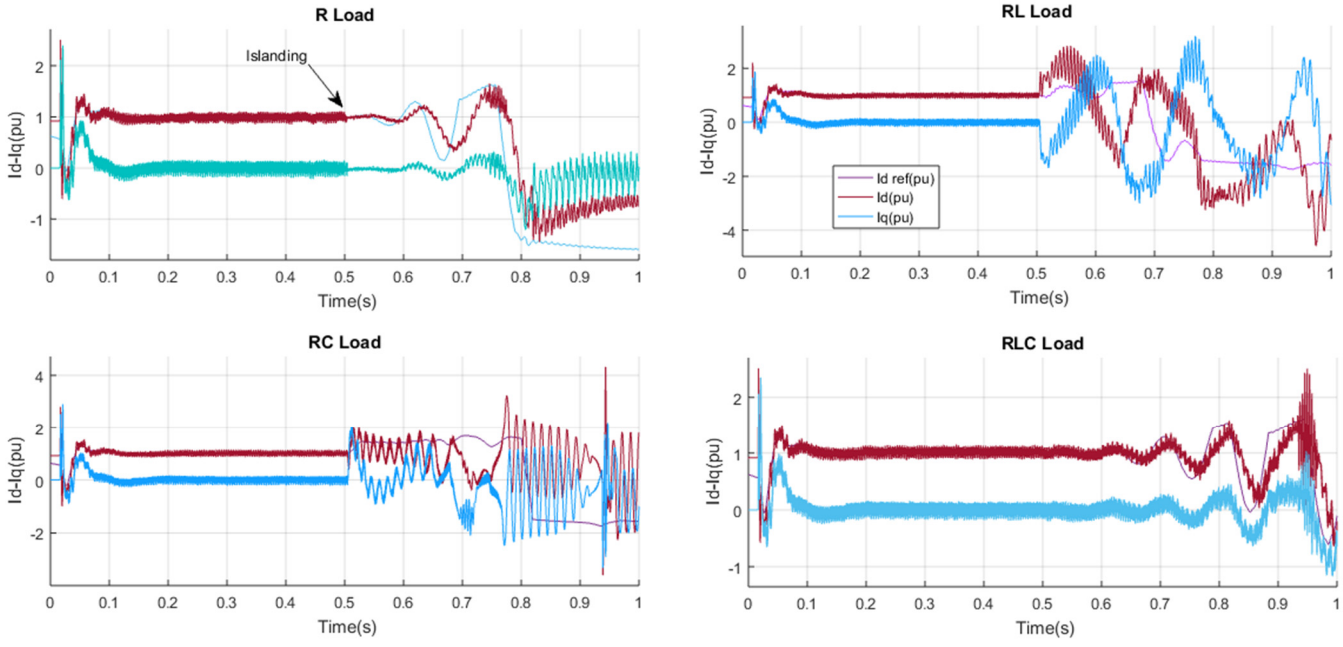


***Fig. 17.*** *$I_d$ and $I_q$ currents variations value of the proposed system in PCC for the case of a) R load, b) RL load, c) RC load, and d) RLC load*

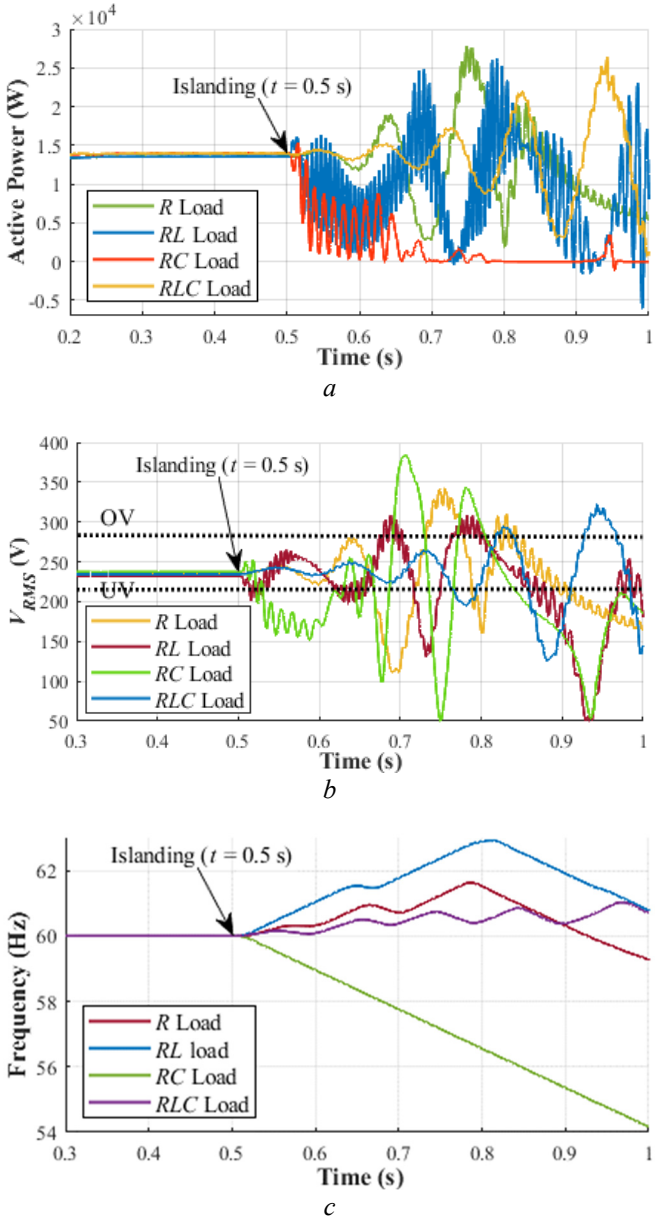


***Fig. 18.*** *Performance of the proposed system in PCC for various load types*
*a* Active power responses,
*b* RMS voltage responses, and
*c* Frequency responses for different load types

stability. As shown in Fig. 18, it can be found that the proposed system can detect the islanding situation perfectly in all cases with a detection time from 53.2 to 649 ms for the VFP method, from 36.6 to 43.4 ms for ROCOF method with purely resistive load, and from 21.3 to 104.1 ms for DC-link method, as shown in Table 7.

### *4.4.2 Effect of Quality Factor Scenario*

The effect of changing the load quality factor on the detection waveform was also investigated. $Q_f$ is defined as the ratio of the reactive power consumption to the rated power output of the DG inverter. IEEE standards require that the islanding detection technique be operational with loads having $1 < Q_f < 2.5$ at the resonant frequency. Fig. 19 shows the

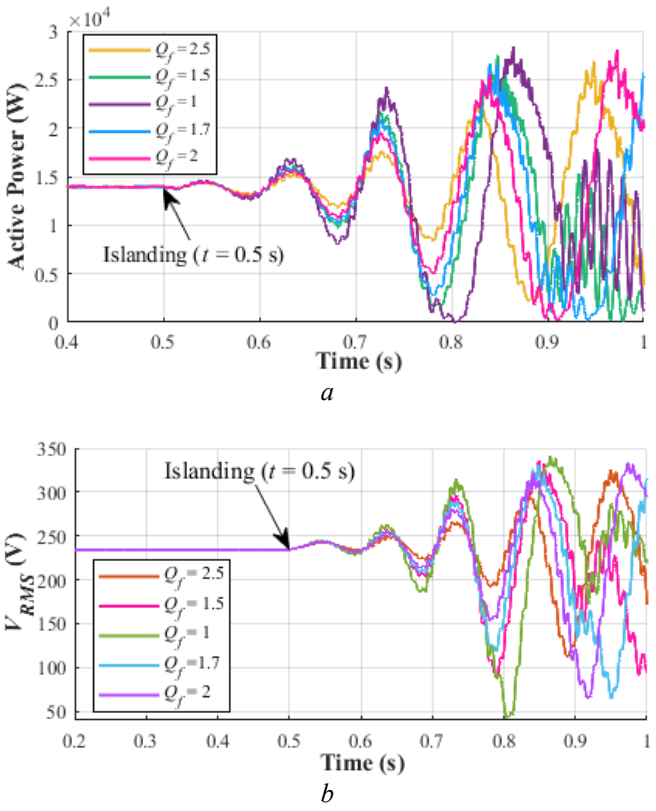


***Fig. 19.*** *Performance of the proposed system at the PCC for RLC load at different $Q_f$ with the UOF/UOV limits:*
*a* Active power, and
*b* RMS voltage

**Table 8** Detection time (ms) of the proposed system with different quality factor and passive IDMs

| Cases | Description | VFP | ROCOF | DC-link |
|---|---|---|---|---|
| 1 | Local load *RLC* with $Q_f = 0.5$ $P_{load} = 14$ kW $Q_L = Q_C = 35$ kVar | 114.3 | 117.1 | 99.2 |
| 2 | Local load *RLC* with $Q_f = 1$ $P_{load} = 14$ kW $Q_L = Q_C = 35$ kVar | 130.7 | 117.8 | 180.4 |
| 3 | Local load *RLC* with $Q_f = 2.5$ $P_{load} = 14$ kW $Q_L = Q_C = 35$ kVar | 148.0 | 119.4 | 185.8 |
| 4 | Local load *RLC* with $Q_f = 1.5$ $P_{load} = 14$ kW $Q_L = Q_C = 35$ kVar | 131.1 | 118.3 | 181.0 |
| 5 | Local load *RLC* with $Q_f = 1.7$ $P_{load} = 14$ kW $Q_L = Q_C = 35$ kVar | 131.2 | 118.5 | 182.1 |
| 6 | Local load *RLC* with $Q_f = 2$ $P_{load} = 14$ kVA $Q_L = Q_C = 35$ kVar | 131.3 | 118.7 | 183.0 |

general effect of changing the $Q_f$ on the output waveform of an island with zero mismatch power imbalance. As it can be seen from Fig. 19, the DG loses its stable operation mode and an islanding condition can be detected by using passive methods under 100 ms, as shown in Table 8.

Fig. 20 presents the frequency and ROCOF during the island condition of the PV system with different local load quality factors, from $Q_f = 1$ to $Q_f = 2.5$, respectively. From Fig. 20, it can be observed the effect of the $Q_f$ on the frequency during islanding condition. In Fig. 20-*a*, the frequency decreases in a very short time. Rapid change in frequency implies a certain variation of ROCOF, as is also presented in [32]. In Fig. 20-*b*, the frequency increases almost in the same speed and the same way. The islanding condition is detected when a ROCOF threshold of 5 Hz/s is exceeded, as depicted in Fig. 20-*b*.

### 4.5 Non-Islanding Event

The evaluation of proposed IDM is also developed for non-islanding disturbances, such as load switching, capacitor switching, and motor starting. The provided algorithm is not activated under the mentioned scenarios. Some tests were carried out and results were obtained according to the following subcases scenario:

#### 4.5.1 Influence of Load Switching Scenario

The common switching of loads leads to changes in electrical parameters. Thus, the performance of islanding is affected by load switching.

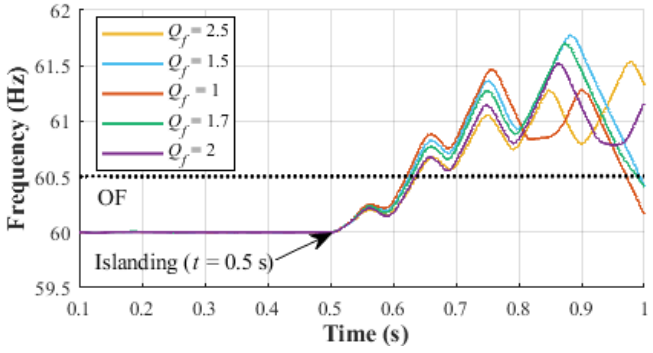


*a*

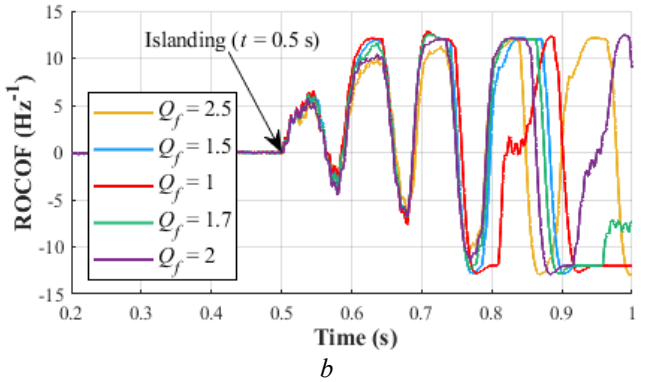


*b*

***Fig. 20.*** *Proposed algorithm during islanding with different $Q_f$ of local load*
*a* Frequency, and
*b* ROCOF

In this case, a sudden load increase is simulated at 0.5 s and a sudden load decrease at 1 s, respectively, to survey the network behaviour under these changes, as can be seen from Fig. 21, where the changes are presented by the zoomed graphs for the active power, and Fig. 22 which shows the frequency and its ROCOF. Both these changes result in some alteration in the output of the proposed detector. However, it will not pass the predefined threshold and accurately separate both scenarios from islanding conditions.

#### 4.5.2 Influence of Capacitor Bank Switching Scenario

In this section, the performance of the proposed algorithm is studied for capacitor bank switching in grid-connected mode to show that the proposed algorithm does not wrong in capacitor bank switching and detect properly the islanding state from capacitor bank switching conditions.

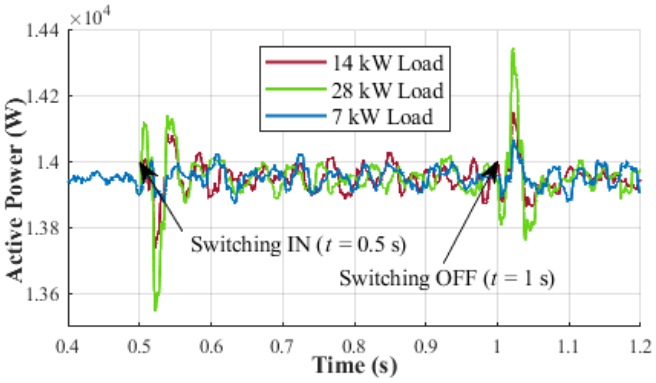


***Fig. 21.*** *Active power for load switching scenario*

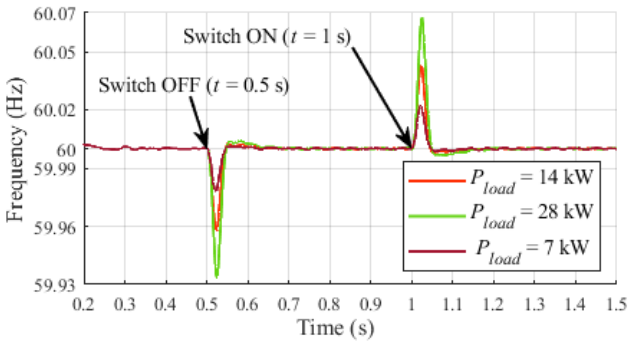


*a*

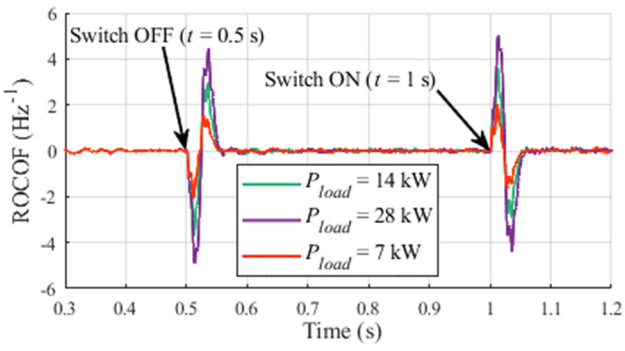


*B*

***Fig. 22****. Frequency and its ROCOF for load switching scenario: a Frequency and b* ROCOF

**Table 9** Performance of the proposed method under different non-islanding events

| Non-islanding scenarios | | Description | Non-islanding performance |
|---|---|---|---|
| Load switching scenario | Case 1 | $P_{load}$ = 7 kW | OK |
| | Case 2 | $P_{load}$ = 14 kW | OK |
| | Case 3 | $P_{load}$ = 28 kW | OK |
| Capacitor switching scenario | Case 1 | $Q_C$ = 28 kVar | OK |
| | Case 2 | $Q_C$ = 20 kVar | OK |
| | Case 3 | $Q_C$ = 10 kVar | OK |
| Motor starting scenario | Case 1 | Motor starting 5050 HP | OK |

Initially, the system works in grid-connected mode. A capacitor bank with 28 kVar reactive power is switched and connected to the system at $t$ = 0.5 s and it is removed at $t$ = 1 s. This operation is repeated for a 10 kVar and 2 kVar load. The capacitors are switched off at $t$ = 1 s to figure out the performance of this proposed system. Fig. 23 shows respectively the $V_{RMS}$, active output power, frequency, and ROCOF of DG. It is clearly identified that the changes in ROCOF do not exceed the threshold value. However, the proposed method treats the load switching as non-islanding.

### *4.5.3 Influence of Induction Motor Starting Scenario*

Fig. 24 presents the (*a*) $V_{RMS}$, (*b*) power, (*c*) frequency, and (*d*) ROCOF under induction motor starting effect and proves that the situation mentioned above regarding the four PV inverters mixed methods remained unchanged during simulation of the proposed algorithm under induction motor starting scenario.

Table 9 summarizes the main points and outcomes from this work under non-islanding situations. Hence, they give a brief picture of the problem which is the performance of the proposed system in non-islanding detection. In this table, the used method succeeded in all the nine studied cases.

### *4.6 Simulation of Multi-System Inverters with Same Methods*

The final case study is a system just like the second case but with four inverter-based PV systems equipped with the same IDMs at the same time.

Compared with the previously proposed studied case, Fig. 25 presents respectively the simulation results for RMS voltage, active power, frequency, and ROCOF for different 6 subcases investigated in this section. Frequency variation (see Fig. 25-*c*) were related directly to the existing active power mismatch (see Fig. 25-*b*) prior to islanding and implicitly to the used IDM, the type of used inverter method, and the grid system associated with them, while voltage was function of the existing reactive power mismatch prior to islanding, used islanding methods, and the inverter's control type [30].

Table 10 presents the obtained detection time of the proposed algorithm compared with the same system when the four inverters used in the system are equipped by the same methods every time also the system is compared with a conventional system without any active methods. This last one failed in detection even by using three different passive methods and that according to their large NDZ. Otherwise, even active methods can sometimes fail in detection like the

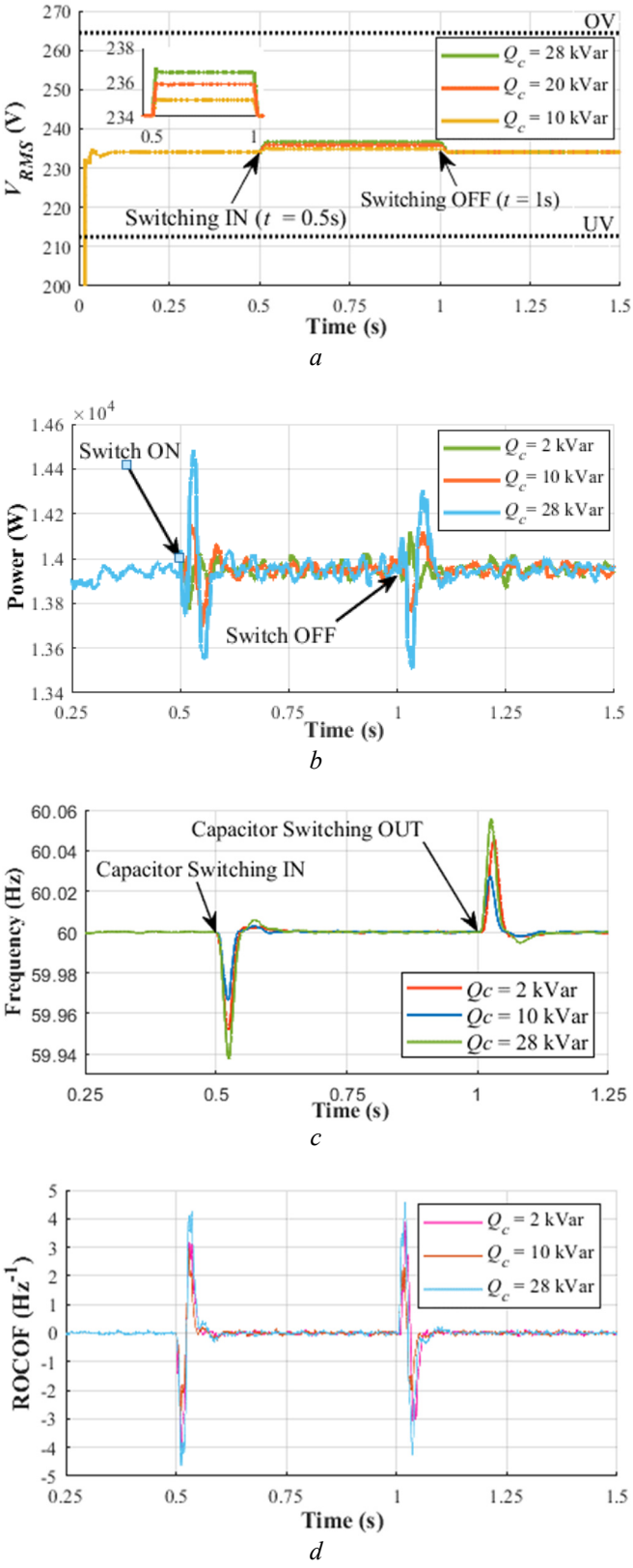


***Fig. 23.*** *Capacitor bank switching scenario*
*a* $V_{RMS}$ voltage
*b* Active power
*c* Frequency
*d* ROCOF

SVS with VFP case. The proposed system gives the shortest detection time in all cases (with VFP, ROCOF, and DC-link) compared with the other cases.

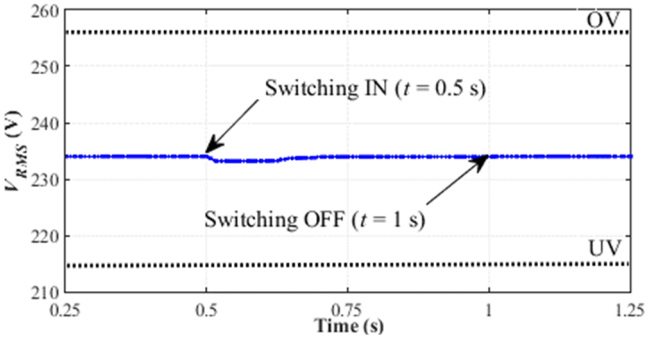


*a*

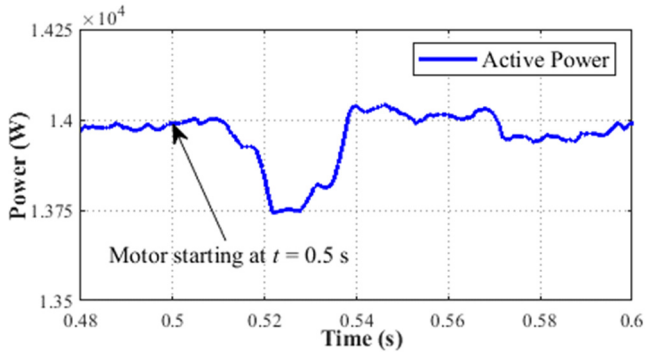


*b*

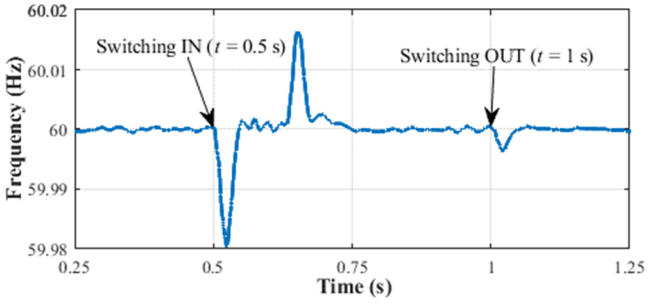


*c*

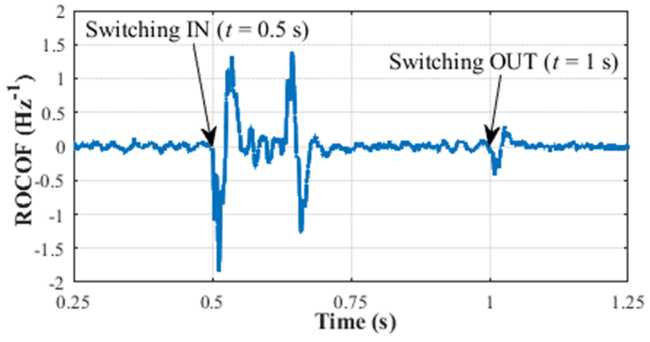


*d*

***Fig. 24.*** *Induction motor starting scenario with the VFP limits: a* $V_{RMS}$ voltage, *b* Active power, *c* Frequency, and d *ROCOF*

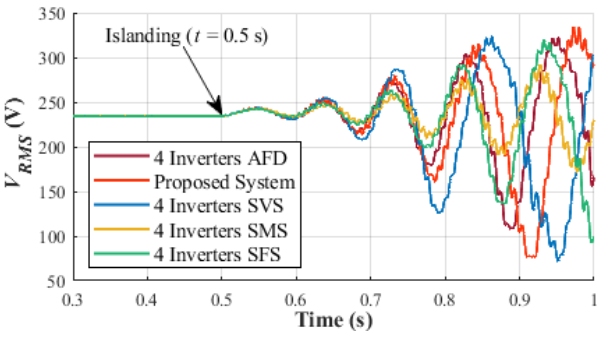


*a*

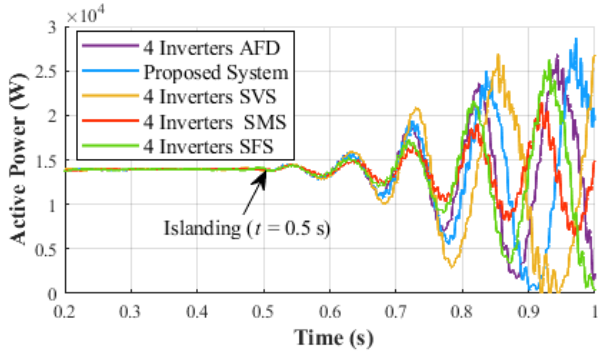


*b*

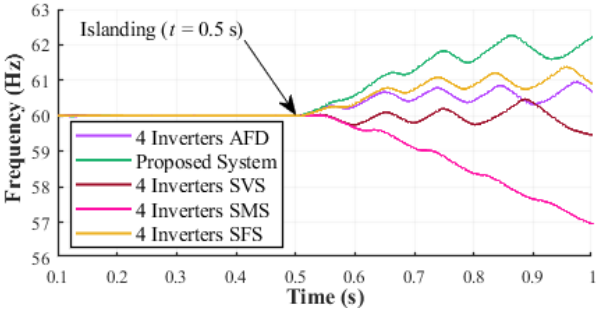


*c*

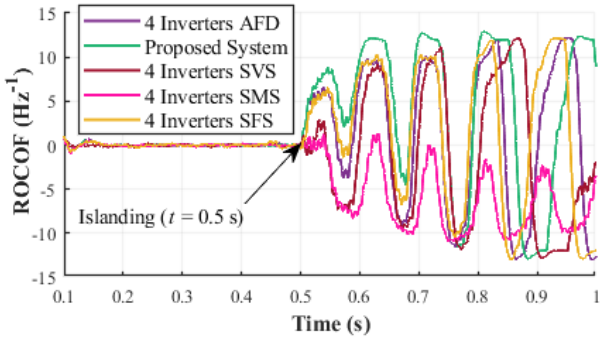


*d*

***Fig. 25.*** *Active power responses applying the same active methods in all inverters for different cases*
*a* $V_{RMS}$ voltage, *b* Active power, *c* Frequency, and *d* ROCOF

### *4.7 Discussion of Obtained Results and Main Achievements*

Overall, the simulation results have verified the efficiency of the proposed method under different operating conditions. The most important factors in islanding protection are the power quality and detection time, which is the lowest amount in the proposed method (147.9 ms in case of VFP method) compared with the methods proposed in [22], where three active IDMs are used in three parallel-connected inverters (529 ms), and [69], where three multi-DG systems are used (255 ms). The proposed system is even more capable to give better detection time if another more performant passive method is applied like ROCOF (119.4 ms).

**Table 10** Detection time (ms) of the proposed system compared with other system using single active methods and passive IDMs

| Description | VFP | ROCOF | DC-link |
|---|---|---|---|
| 4 SMS inverters | 253.2 | 325.8 | 275.0 |
| 4 SFS inverters | 181.9 | 201.9 | 191.1 |
| 4 SVS inverters | - | 120.6 | 188.8 |
| 4 AFD inverters | 198.5 | 135.7 | 193.5 |
| System without methods | - | - | - |
| Proposed system | **147.9** | **119.4** | **185.6** |

The proposed algorithm is faster than other well-known methods used for islanding detection. The average detection rate for the proposed IDM is less than 100 ms which is considerably smaller than other existing methods applied into multi-inverter systems in the literature as [22, 39] and [69]. The proposed algorithm also exceeds the systems using similar active methods (e.g., scenario 10 with the same active method in each inverter, where the detection time is always better in the proposed method). The system also has good and acceptable power quality compared with [22] and [69].

The proposed method results in a low computational burden [42, 46] in comparison with remote and intelligent IDMs [43] or advanced passive IDMs [48], which makes it suitable for implementation in large-scale power systems. In addition, compared to other passive methods like [20, 46-48], the NDZ is significantly reduced. In general, any change in the power grid that affects the voltage of load at the PCC can be identified and separated from the islanding conditions.

From Fig. 26, since among the six investigated subcases, four out subcases showed reliable islanding results, while two subcases, it is about the system with four DG inverters equipped with four similar SVS methods and the system without any detection method, which failed to satisfy the standard islanding operating conditions. Among the investigated subcases in this section, the proposed system had the best islanding response, while the case of a system with four SMS methods had the longest response time. Moreover, the load had an impact on the system frequency response (see Fig. 25-*c*) prior to islanding and that was obvious in the subcases presented before while voltage variation had a direct impact on load behaviour.

## 5 Conclusion

In this paper, a new hybrid IDM for GCPVSs is proposed. The proposed system performance has been studied under different conditions such as load switching and loads with low- and high-quality factor, changes in solar radiation, capacitor switching, induction motor starting, various power tests such as much higher or less than DG power, with different systems applying the same active methods or even without any active methods. From the simulation studies, it can be concluded that the proposed system is exact and quick enough to identify the islanding event inside the 2 s required in the standards and grid codes in all studied conditions. Likewise, as a final point, the proposed system has a generally low impact on the system power quality factor. Based on numerical simulation results, it is shown that the proposed system under the proposed combination methods (proposed system combination IDMs) is capable of islanding detection within the minimum standard time for loads with different quality factors and under diverse scenarios and conditions.

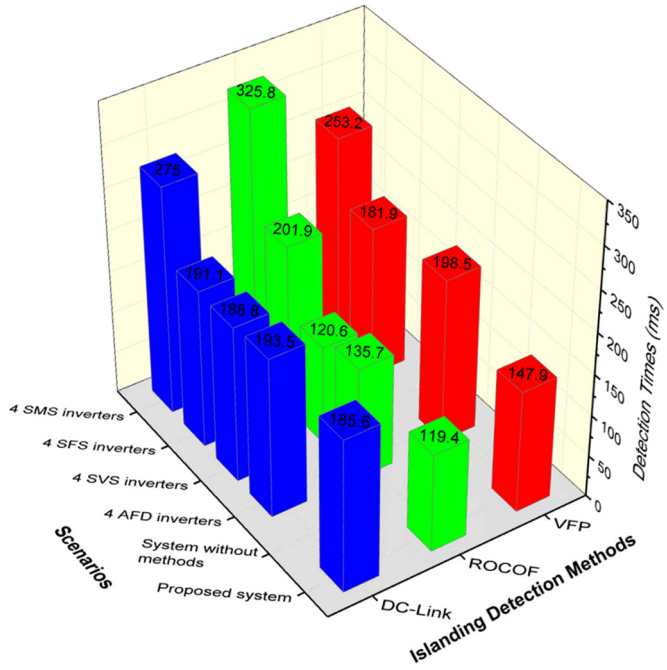


***Fig. 26.*** *Detection time using the same active methods in all inverters for different cases using passive methods*

## 6 Acknowledgement

This work was supported by VILLUM FONDEN under the VILLUM Investigator Grant (no. 25920): Center for Research on Microgrids (CROM); www.crom.et.aau.dk

## 7 References

[1] IEEE Std. 929-2000: 'IEEE Recommended Practice for Utility Interface of Photovoltaic (PV) Systems', 2000

[2] Deshbhratar, P., Somalwr, R., Kadwane, S.G.: 'Comparative analysis of islanding detection methods for multiple DG based system'. Int. Conf. Elect., Electron., and Optimization Techn. (ICEEOT), IEEE, 2016, pp. 1525-1530

[3] Banu, I.V., Istrate, M., Machidon, D., et al.: 'A study on anti-islanding detection algorithms for grid-tied photovoltaic systems'. 2014 Int. Conf. Optimization Elect. and Electron. Equipment (OPTIM), 2014, pp. 655-660

[4] Zhihong,Y., Kolwalkar, A., Zhang, Y., et al.: 'Evaluation of anti-islanding schemes based on nondetection zone concept', IEEE Trans. Power Electron., 2004, 19, (5), pp. 1171-1176

[5] Wang, X., Freitas, W., Xu, W.: 'Dynamic non-detection zones of positive feedback anti-islanding methods for inverter-based distributed generators,' IEEE Trans. Power Del., 2011, 26, (2), pp. 1145-1155

[6] Arulkumar, K., Vijayakumar, D., Palanisamy, K.: 'Recent advances and control techniques in grid connected PV system–A review,' Int. J. Renewable Energy Res., 2016, 6, (3), pp. 1037-1049

[7] Eltawil, A., Zhao, Z.: 'Grid-connected photovoltaic power systems: Technical and potential problems – A review,' Renewable Sustain. Energy Rev., 2010, 14, (1), pp. 112-129

[8] Zhang, X., XIE, D.: 'Performance Assessment of Islanding Detection for Multi-Inverter Grid-connected Photovoltaic Systems', Energy Power Eng., 2013, 5, (4), pp. 1517-1520
[9] Aman, M., Jasmon, B., Mokhlis, B., et al.: 'Modeling and simulation of digital frequency relay for generator protection'. IEEE Int. Conf. Power and Energy, 2012, pp. 701-706
[10] Chen, K., Wang, Y., Tian, S., et al.: 'Interference of various active islanding detection methods with positive feedback in multi-inverter power system', J. Renewable Sustain. Energy, 2015, 7, (3), 033103
[11] Liu, F., Kang, Y., Zhang, Y., et al.: 'Improved SMS islanding detection method for grid-connected converters,' IET Renewable Power Generation, 2010, 4, (1), pp. 36-42
[12] Hatata, A.Y., Abd-Raboh, El-H., Sedhom, et al.: 'Proposed Sandia frequency shift for anti-islanding detection method based on artificial immune system', Alexandria Eng. J., 2018, 57, (1), pp. 235-245
[13] Schutz, D., Ropp, M.: 'Simulation and experimental study of multi-inverter islanding'. 2011 IEEE Power and Energy Soc. General Meeting, IEEE, 2011. pp. 1-5
[14] Skocil, T., Gomis-Bellmunt, O., Montesinos-Miracle, D., et al.: 'Passive and active methods of islanding for PV systems'. 2009, EPE'09, 13th European Conf. Power Electron. and Applicat., IEEE, 2009, pp. 1-10
[15] Laghari, A., Mokhlis, H., Karimi, M., et al.: 'Computational Intelligence based techniques for islanding detection of distributed generation in distribution network: A review', Energy Convers. Manage., 2014, 88, pp. 139-152
[16] Aghdam, T.S., Karegar, H.K.: 'Settings of ROCOF relays for islanding detection of wind turbine'. 2011 Int. Conf. Adv. Power Syst. Autom. and Protection (APAP), IEEE, 2011, pp. 1402-1405
[17] Nassif, A., Madsen, C.: 'A real case application of ROCOF and vector surge relays for anti-islanding protection of distributed energy resources'. 2017 IEEE Elect. Power and Energy Conf. (EPEC), IEEE, Oct. 2017, pp. 1-5
[18] Freitas, W., Xu, W., Affonso, C.M., et al.: 'Comparative analysis between ROCOF and vector surge relays for distributed generation applications', IEEE Trans. Power Del., 20, (2), 2005, pp. 1315-1324
[19] Report IEA PVPS T5-09., 'Evaluation of islanding detection methods for photovoltaic utility-interactive power systems', 2002
[20] Raza, S., Arof, H., Mokhlis, H., et al.: 'Passive islanding detection technique for synchronous generators based on performance ranking of different passive parameters', IET-GTD, 11, (17), 2017, pp. 4175-4183
[21] Lopes, A., Sun, H.: 'Performance assessment of active frequency drifting islanding detection methods', IEEE Trans. Energy Convers., 2006, 21, (1), pp. 171-180
[22] El-Moubarak, M., Hassan, M., Faza, A.: 'Performance of three islanding detection methods for grid-tied multi-inverters'. 2015 IEEE 15th Int. Conf. Environment and Elect. Eng. (EEEIC), IEEE, 2015, pp. 1999-2004
[23] Ropp, E., Begovic, M., Rohatgi, A.: 'Analysis and performance assessment of the active frequency drift method of islanding prevention', IEEE Trans. Energy Convers., 1999, 14, (3), pp. 810-816
[24] Hong, Y., Huang, W.: 'Investigation of Frequency drift methods of Islanding Detection with multiple PV inverters'. Int. Conf. and Expo. Electron. and Appl., 2014, pp. 429-434
[25] Yu, B.: 'An improved active frequency drift anti-islanding method for multiple PV micro-inverter systems'. IEICE Electron. Exp., 2014, 11, (6), p. 20140143
[26] Yu, B., Matsui, M., Yu, G.: 'A review of current anti-islanding methods for photovoltaic power system', Solar Energy, 2010, 84, (5), pp. 745-754
[27] Kamyab, E., Sadeh, J.: 'Islanding detection method for photovoltaic distributed generation based on voltage drifting', IET Generation, Transmission & Distribution, 7, (6), pp. 584-592
[28] Khamis, A., Shareef, H., Mohamed, A., et al.: 'Islanding detection in a distributed generation integrated power system using phase space technique and probabilistic neural network', Neurocomputing, 2015, 148, pp. 587-599
[29] Yu, B., Matsui, M., Jung, Y., et al.: 'Modeling and design of phase shift anti-islanding method using non-detection zone', Solar Energy, 2017, 81, (11), pp. 1333-1339
[30] Bignucolo, F., Cerretti, A., Coppo, M., et al.: 'Impact of distributed generation grid code requirements on islanding detection in LV networks', Energies, 2017, 10, (2), pp. 156
[31] Xu, M., Melnik, V., Borup, U.: 'Modeling anti-islanding protection devices for photovoltaic systems', Renewable Energy, 2004, 29, (15), pp. 2195-2216
[32] Banu, I.V., Istrate, M.: 'Islanding prevention scheme for Grid-Connected Photovoltaic systems in Matlab/Simulink'. 2014 49th Int. Universities Power Eng. Conf. (UPEC), 2014, pp. 1-6
[33] Hovanessian, A., Norouzi, M.A.: 'Islanding detection using wavelet transform and rate of change of frequency relay method in presence of different distributed generation technologies', IEEJ Trans. Elect. Electron. Eng., 2016, 11, p. S68
[34] Ropp, E., Begovic, M., Rohatgi, A.: 'Prevention of islanding in grid connected photovoltaic systems', Progress Photovolt.: Res. Appl., 1999, 7, (1), pp. 39-59
[35] Abdelsalam, K., Massoud, M., Ahmed, S., et al.: 'High-performance adaptive perturb and observe MPPT technique for photovoltaic-based microgrids', IEEE Trans. Power Electron., 2011, 26, (4), pp. 1010-1021
[36] Ghalavand, F., Alizade, B.A.M., Gaber, H., et al.: 'Microgrid islanding detection based on mathematical morphology', Energies, 2018, 11, (10), p. 2696
[37] The MathWorks, Inc., 'Single-Phase, 240 Vrms, 3500 W Transformerless Grid-Connected PV Array', https://www.mathworks.com/help/physmod/sps/examples/single-phase-240-vrms-3500-w-transformerless-grid-connected-pv-array.html, accessed 22 September 2019
[38] Zeineldin, H.H., El-Saadany, E.F., Salama, M.M.A.: 'Impact of DG interface control on islanding detection and nondetection zones', IEEE Trans. Power Del., 2006, 21, (3), pp. 1515-1523
[39] Liu, S., Zhuang, S., Xu, Q., et al.: 'Improved voltage shift islanding detection method for multi-inverter grid-connected photovoltaic systems', IET-GTD, 2016, 10, (13), pp. 3163-3169

[40] Akhlaghi, S., Ghadimi, A.A., Akhlaghi, A.: 'A novel hybrid islanding detection method combination of SMS and Q-f for islanding detection of inverter- based DG'. 2014 Power and Energy Conf. Illinois (PECI), 2014, pp. 1-8

[41] Mlakić, D., Baghaee, H.R., Nikolovski, S.: 'Gibbs Phenomenon-Based Hybrid Islanding Detection Strategy for VSC-Based Microgrids Using Frequency Shift, $THD_U$, and $RMS_U$', IEEE Trans. Smart Grid, 2019, 10, (5), pp. 5479-5491

[42] Mlakić, D., Baghaee, H.R., Nikolovski, S.: 'A Novel ANFIS-Based Islanding Detection for Inverter-Interfaced Microgrids', IEEE Trans. Smart Grid, 2019, 10, (4), pp. 4411-4424

[43] Kim, M. S., Haider, R., Cho, G. J., et al.: 'Comprehensive Review of Islanding Detection Methods for Distributed Generation Systems', Energies, 2019, 12, (5), p. 837

[44] Manikonda, S.K.G., Gaonkar, D.N., 'Comprehensive review of IDMs in DG systems', *IET Smart Grid*, 2019, 2, (1), pp. 11-24

[45] Dutta, S., Sadhu, P.K., Reddy, M.J., et al.: 'Shifting of research trends in islanding detection method - a comprehensive survey', Prot Control Mod Power Syst, 2018, 3, (1), pp. 1-20

[46] Haider, R., Kim, C.H., Ghanbari, T., et al.: 'Passive islanding detection scheme based on autocorrelation function of modal current envelope for PV units', IET-GTD, 2018, 12, (3), pp. 726-736

[47] Gupta, N., Garg, R.: 'Algorithm for islanding detection in photovoltaic generator network connected to low-voltage grid', IET Generation, Transmission & Distribution, 2018, 12, (10), pp. 2280-2287

[48] Reddy, V. R., Sreeraj, E. S., 'A Feedback-Based Passive Islanding Detection Technique for One-Cycle-Controlled Single-Phase Inverter Used in Photovoltaic Systems', IEEE Trans. Ind. Electron., 2020, 67, (8), pp. 6541-6549

[49] Bakhshi, R., Sadeh, J.: 'Voltage positive feedback based active method for islanding detection of PV system with string inverter using sliding mode controller', Solar Energy, 2016, 137, pp. 564-577

[50] Shrivastava, S., Jain, S., Nema, R.K., et al.: 'Two level islanding detection method for distributed generators in distribution networks', Int. J. Elect. Power & Energy Systems, 2017, 87, pp. 222-231

[51] Yafaoui, A., Wu, B., Kouro, S.: 'Improved Active Frequency Drift Anti-islanding Detection Method for Grid Connected PV Systems', *IEEE Trans. Power Electron.*, 2012, 27, (5), pp. 2367-2375

[52] Velasco, D., Trujillo, C., Garcera, G., et al., 'An Active Anti-Islanding Method Based on Phase-PLL Perturbation', IEEE Trans. Power Electron., 2011, 26, (4), pp. 1056-1066

[53] Padmanaban, S., Priyadarshi, N., Bhaskar, M.S., et al.: 'A Hybrid ANFIS-ABC Based MPPT Controller for PV System With Anti-Islanding Grid Protection: Experimental Realization', *IEEE Access*, 2019, 7, pp. 103377-103389

[54] Ke, J., Zhengxuan, Z., Qijuan, Z., et al.: 'Islanding detection method of multi-port photovoltaic DC micro grid based on harmonic impedance measurement', IET Renewable Power Generation, 2019, 13, (14), pp. 2604-2611

[55] Malakondaiah, M., Boddeti, K.K., Naidu, B. R., et al.: 'Second harmonic impedance drift-based islanding detection method', IET-GTD, 2019, 13, (23), pp. 5313-5324

[56] Chen, X., Li Y., Crossley, P.: 'A Novel Hybrid Islanding Detection Method for Grid-Connected Microgrids With Multiple Inverter-Based Distributed Generators Based on Adaptive Reactive Power Disturbance and Passive Criteria', IEEE Trans. Power Electron., 2019, 34, (9), pp. 9342-9356

[57] Murugesan, S., Murali, V.: 'Hybrid Analyzing Technique Based Active Islanding Detection for Multiple DGs', IEEE Trans. Ind. Informat., 2019, 15, (3), pp. 1311-1320

[58] Mishra, M., Sahani, M., Rout, P.K.: 'An islanding detection algorithm for distributed generation based on Hilbert–Huang transform and extreme learning machine', Sustain. Energy, Grids Netw., 2017, 9, pp. 13-26

[59] Rostami, A., Jalilian, A., Hagh, M. T., et al.: 'Islanding Detection of Distributed Generation Based on Rate of Change of Exciter Voltage With Circuit Breaker Switching Strategy', IEEE Trans. Ind. Appl., 2019, 55, (1), pp. 954-963

[60] Nale, R., Biswal, M., Kishor, N.: 'Transient Component Based Approach for Islanding Detection in Distributed Generation', IEEE Trans. Sustain. Energy, 2019, 10, (3), pp. 1129-1138

[61] Nikolovski, S., Baghaee H.R., Mlakić, D.: 'Islanding Detection of Synchronous Generator-Based DGs using Rate of Change of Reactive Power', IEEE Syst. J., 2019, 13, (4), pp. 4344-4354

[62] Baghaee, H.R., Mlakić, D., Nikolovski S., et al.: 'Anti-Islanding Protection of PV-Based Microgrids Consisting of PHEVs Using SVMs', IEEE Trans. Smart Grid, 2020, 11, (1), pp. 483-500

[63] Yu, B., Matsui, M., Yu, G.: 'A Correlation-Based Islanding-Detection Method Using Current-Magnitude Disturbance for PV System', IEEE Trans. Ind. Electron., 2011, 58, (7), pp. 2935-2943

[64] Wang, M.H., Huang, M., Liou, K.: 'Islanding detection method for grid connected photovoltaic systems', IET Renewable Power Generation, 2015, 9, (6), pp. 700-709

[65] Das, P.P., Chattopadhyay, S.: 'A Voltage-Independent Islanding Detection Method and Low-Voltage Ride Through of a Two-Stage PV Inverter', IEEE Trans. Ind. Appl., 2018, 54, (3), pp. 2773-2783

[66] Khodaparastan, M., Vahedi, H., Khazaeli, F., et al.: 'A Novel Hybrid Islanding Detection Method for Inverter-Based DGs Using SFS and ROCOF', IEEE Trans. Power Del., 2017, 32, (5), pp. 2162-2170

[67] Estébanez, E. J., Moreno, V.M., Pigazo, A., et al.: 'Performance Evaluation of Active Islanding-Detection Algorithms in Distributed-Generation Photovoltaic Systems: Two Inverters Case', IEEE Trans. Ind. Electron., 2011, 58, (4), pp. 1185-1193

[68] Trujillo, C., Velasco, D., Figueres, E., et. al.: 'Local and Remote Techniques for Islanding Detection in Distributed Generators', in Gaonkar, D.N. (Ed.): 'Distributed Generation'. (IntechOpen, Rijeka, 2010, 6), pp. 119-140

[69] Cardenas, A., Agbossou, K., Doumbia, M.: 'Islanding Detection Method for Multi-Inverter Distributed Generation', J. Electromagn. Anal. Appl., 2009, 1, (3), pp. 170-180

[70] Ropp, M.E., Begovic, M., Rohatgi, A., et al.: 'Determining the relative effectiveness of islanding detection methods using phase criteria and nondetection zones', IEEE Trans. Energy Conv., 2000, 15 (3), pp. 290-296

[71] Kim, B.H., Sul, S. K.: 'Analysis of non detection zone for multiple distributed PCS based on equivalent single PCS using reactive power approach'. in 2016 IEEE Appl. Power Electron. Conf. and Exp. (APEC), 2016, pp. 1220-1226

[72] Sun, H., Lopes, L.A.C., Luo, Z.: 'Analysis and comparison of islanding detection methods using a new load parameter space'. 30th Annu. Conf. IEEE Ind. Electron. Soc. (IECON), 2004, 2, pp. 1172-1177

[73] Lashab, A., Sera, D., Guerrero, J. M., et al.: 'Discrete Model-Predictive-Control-Based Maximum Power Point Tracking for PV Systems: Overview and Evaluation', IEEE Trans. Power Electron., 2018, 33, (8), pp. 7273-7287

[74] Abouadane, H., Fakkar, A., Sera, D., et al.: 'Multiple-Power-Sample Based P&O MPPT for Fast-Changing Irradiance Conditions for a Simple Implementation', IEEE J. Photovolt., 2020, 10, (5), pp. 1481-1488

## 8 Appendices

Formulas for the analysis of NDZ:

$$\begin{aligned} I_{inv\_con} &= I_{inv_{AFD}} + I_{inv_{SMS}} + I_{inv_{SFS}} + I_{inv_{SVS}} \\ &= I_{AFD+SMS} + I_{SFS+SVS} \\ &= \omega_1 \sin(\omega t + \theta_{AFD}) \\ &+ \omega_2 \sin(\omega t + \theta_{SMS}) \\ &+ \omega_3 \sin(\omega t + \theta_{SFS}) \\ &+ \omega_4 \sin(\omega t + \theta_{SVS}) \end{aligned} \quad (11)$$

$$\begin{aligned} I_{AFD+SMS} &= \sqrt{(2\omega^2[1 + \cos(\theta_{AFD})\cos(\theta_{SMS}) + \sin(\theta_{AFD})\sin(\theta_{SMS})])} \\ &\cdot \sin\left(\omega t + \tan^{-1}\left(\frac{\sin(\theta_{AFD}) + \sin(\theta_{SMS})}{\cos(\theta_{AFD}) + \cos(\theta_{SMS})}\right)\right) \\ &= A\sin(\omega t + \varphi_1) \end{aligned} \quad (12)$$

$$\begin{aligned} I_{SFS+SVS} &= \sqrt{(2 \cdot \omega^2[1 + \cos(\theta_{SFS})\cos(\theta_{SVS}) + \sin(\theta_{SFS})\sin(\theta_{SVS})])} \\ &\cdot \sin\left(\omega t + \tan^{-1}\left(\frac{\sin(\theta_{SFS}) + \sin(\theta_{SVS})}{\cos(\theta_{SFS}) + \cos(\theta_{SVS})}\right)\right) \\ &= B\sin(\omega t + \varphi_2) \end{aligned} \quad (13)$$

$$\begin{aligned} I_{inv-conv} &= A\sin(\omega t + \varphi_1) + B\sin(\omega t + \varphi_2) \\ &= \sqrt{[A\cos(\varphi_1) + B\cos(\varphi_2)]^2 + [A\sin(\varphi_1) + B\sin(\varphi_2)]^2} \\ &\cdot \sin\left(\omega t + \tan^{-1}\frac{A\sin(\varphi_1) + B\sin(\varphi_2)}{A\cos(\varphi_1) + B\cos(\varphi_2)}\right) \\ &= C\sin\left(\omega t + \varphi_{inv_{conv}}\right) \end{aligned} \quad (14)$$